Groundwater for Sustainable Development 28 (2025) 101396

Contents lists available at ScienceDirect

Groundwater for Sustainable Development

journal homepage: www.elsevier.com/locate/gsd

Research paper

Sustainable restoration of low-quality groundwater through aquifer storage and recovery

Vahid Sobhi Gollo [a,*,1], Bentley Bo Schmidt [a,b,1], Carsten Hansen [b], Nima Shokri [a,c,**]

[a] Institute of Geo-Hydroinformatics, Hamburg University of Technology, 21073, Hamburg, Germany
[b] Consulaqua Beratungsgesellschaft mbH, 20539, Hamburg, Germany
[c] United Nations University Hub on Engineering to Face Climate Change at the Hamburg University of Technology, United Nations University Institute for Water, Environment and Health (UNU-INWEH), Hamburg, Germany

HIGHLIGHTS

- ASR enhances storage capacity and water quality in sulphate-rich aquifers.
- Abandoned wells can be repurposed for sustainable ASR use.
- Seasonal ASR storage can help mitigate urban water scarcity.
- Numerical modeling to optimize ASR in non-compliant aquifers.
- Developed a framework identifying factors affecting ASR recovery efficiency.

GRAPHICAL ABSTRACT

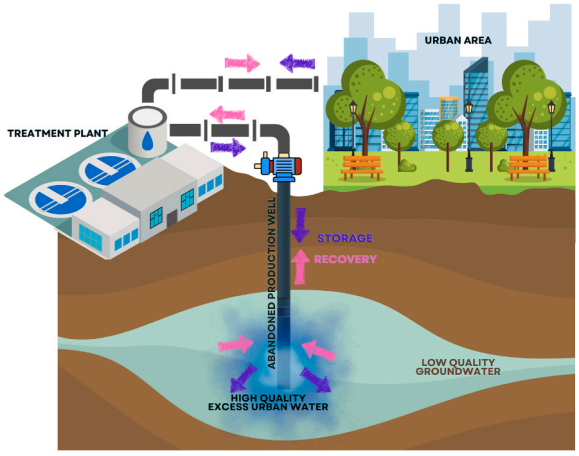

ARTICLE INFO

Keywords:
Sustainable water management
Aquifer storage and recovery (ASR)
Hydrogeological parameters
Retrofitting inactive production wells
Groundwater contamination mitigation

ABSTRACT

The escalating challenges in urban water supply, driven by rapid urbanization, climate change, and water resources pollution, necessitate innovative solutions for sustainable water management. Urban areas frequently encounter spatial constraints for the installation of new production wells, thereby intensifying water scarcity. Shifting climate conditions lead to increased occurrences of extreme weather events, aggravating global water scarcity and impeding sustainable development, particularly impacting human health and exacerbating societal inequalities. To address this issue, our study explores the retrofitting of inactive production wells for aquifer storage and recovery (ASR) in low-quality aquifers, providing a systematic framework. The evaluation focuses on the suitability of inactive wells for ASR operations and utilizes the FEFLOW 8.1 groundwater model to assess the impact of hydrogeological conditions on ASR system recovery efficiency (RE). To validate this framework, we

* Corresponding author.
** Corresponding author. Institute of Geo-Hydroinformatics, Hamburg University of Technology Am Schwarzenberg-Campus 3 (E), 21073 Hamburg, Germany.
E-mail addresses: vahid.sobhi.gollo@tuhh.de (V. Sobhi Gollo), nima.shokri@tuhh.de (N. Shokri).
[1] Author Contributions: V.S.G. and B.S. contributed equally to this work.

https://doi.org/10.1016/j.gsd.2024.101396
Received 21 December 2023; Received in revised form 7 December 2024; Accepted 15 December 2024
Available online 18 December 2024

concentrate on the northwest region of the Hamburg metropolitan area, utilizing generalized hydrogeological conditions to yield universally applicable results. This region is characterized by high sulphate concentrations in groundwater, limiting the utility of production wells. Our findings demonstrate that ASR in a low-quality aquifer can constitute a viable strategy to address water scarcity. Under ideal aquifer conditions, ASR can achieve recovery efficiencies exceeding 100%. Our proposed framework emphasizes the necessity of a meticulous assessment of well design, considering construction materials and geological factors to prevent clogging. Key efficiency factors include the hydraulic gradient, injection and ambient concentrations, proximity to production wells, and dispersivity. Furthermore, ASR contributes to cost reduction by enhancing water management infrastructure and optimizing capacity utilization. This research provides a comprehensive perspective, offering valuable insights applicable to diverse locations grappling with water scarcity challenges.

1. Introduction

The significance of water in preserving ecological systems (Postel, 2000), human communities (Jéquier and Constant, 2010), and agricultural productivity (Mannan et al., 2018; Pimentel et al., 2004) is emphasized by its central role within the framework of the Sustainable Development Goals (SDGs) established by the UN General Assembly (UN General assembly resolution, September 2015), which aim to promote global prosperity and well-being through sustainable development and environmental stewardship. According to the Global Sustainable Development Report (United Nations, 2023), the lack of access to safe water and sanitation remains a critical issue for billions of people. Inadequate access to clean water and sanitation facilities, coupled with the risk of water pollution from hazardous chemicals, contributes to the prevalence of diseases such as cholera, diarrhea, dysentery, hepatitis A, typhoid, and polio (Ashbolt, 2004; WHO, 2023; Alcamo, 2019). Moreover, climate change can exert significant pressure on water resources (Aminzadeh et al., 2024), resulting in increased frequency of droughts, intensified rainfall patterns (Dillon, 2009; Williams and O'Gorman, 2022), more frequent and intense stormwater events, and elevated temperatures leading to increased evapotranspiration rates (Hajek and Knapp, 2022; Williams and O'Gorman, 2022; Aminzadeh et al., 2023). These multifaceted impacts collectively diminish the quality and quantity of the freshwater resources, especially affecting the capacity of shallow aquifers (Dillon, 2009; Dillon et al., 2019a) which are generally considered as self-purified source of water supply (Lall et al., 2020). Developing resilient and efficient water infrastructure is essential to mitigate the severe effects of climate change (Kumar et al., 2020). Improving water management can alleviate the adverse impacts of water stress on social, economic, and environmental aspects (Bhaduri et al., 2016).

Exhibiting resilience to pollution and climate-induced alterations in contrast to surface water sources and shallow aquifers, deep aquifers hold substantial potential for future water supply (Dillon et al., 2019b; Goderniaux et al., 2015; Goel, 2021). Nonetheless, an effective and sustainable management of these aquifers is imperative to harness the full potential of this groundwater resource (Velis et al., 2017).

An increasingly employed method for the maintenance, enhancement, and safeguarding of stressed groundwater systems is Managed Aquifer Recharge (MAR) (Pyne, 1995; Dillon et al., 2019a). This technique is defined as the deliberate replenishment of aquifers with water, with the aim of subsequent recovery or environmental benefit (Seiler and Gat, 2007; Dillon, 2009). In contrast to unintentional and unmanaged aquifer recharge methods, which encompass processes such as water leakage from pipes and sewers, stormwater drainage into wells and sumps, removal of deep-rooted vegetation, soil tillage for the disposal of excess water without consideration for reuse, or the discharge of water from mining and industrial operations into sumps, MAR is achieved through controlled practices such as streambed channel modifications, bank filtration, water spreading, recharge wells and shafts, and controlled reservoir releases (NRMMC, EPHC, and NHMRC, 2009).

An increasing array of methodologies is being employed globally for MAR. Tuinhof and Heederik (2002) have catalogued numerous MAR projects of diverse nature on a global scale. The International Groundwater Resources Assessment Centre (IGRAC) has established an online MAR inventory comprising 1200 case studies from around the world (Stefan and Ansems, 2018). A coherent description of various MAR systems (see supplementary materials, Table S1) is presented by Dillon (2009) and Dillon et al. (2022). The applicability of each of 13 techniques mentioned in Dillon's description, is contingent upon regional hydrogeological conditions, topographical features, the quality of water sources, and requisites for water resource management (Maliva, 2020).

Among these, the method known as "Aquifer Storage and Recovery" (ASR) is used for the purpose of storing water within a suitable aquifer through a single well during periods of water availability and subsequently recovering the stored water from the same well as needed (Pyne, 1995). ASR typically involves the use of a single well, serving both injection and recovery functions, which is often more economically advantageous compared to the utilization of separate wells for these distinct purposes. However, in certain operational scenarios, the preference may arise for the deployment of separate wells for injection and recovery (Pyne, 1995).

ASR emerges as a promising method for addressing various challenges outlined in the Sustainable Development Goals (SDGs; United Nations, 2023), ensuring access to clean water (SDG 6: Clean Water and Sanitation). ASR presents a valuable option, particularly in densely populated urban areas where space is limited (Pyne, 1995). This technique enables communities to efficiently store surplus water during the rainy season and retrieve it during periods of scarcity, thereby ensuring a consistent supply of water. Nonetheless, the applicability of ASR varies, and simpler albeit less efficient systems such as surface spreading methods remain available (Zheng et al., 2021).

ASR can be effectively employed in saline or brackish aquifers (Reese, 2002), minimizing treatment requirements and enhancing infrastructure utilization efficiency (Brown, 2005). Moreover, ASR plays a pivotal role in addressing SDG 10: Reduce Inequalities. ASR projects are viable in both urban (Reese, 2002) and rural (Taneja and Khepar, 1996) settings, thereby bridging the gap in water access between different communities. For instance, Indian farmers have successfully repurposed production wells (cavity wells) for ASR in saline aquifers to store rainwater for irrigation purposes, leveraging underground treatment methods (Malik et al., 2006; Taneja and Khepar, 1996). In addition, similar methods have been implemented in the Mediterranean region, such as in the Los Arenales aquifer in Spain, where ASR has been used since the early 2000s to alleviate the impacts of drought and water scarcity (Henao Casas et al., 2022). Such initiatives have the potential to alleviate competition for drinking water resources. Similar projects could be replicated in suitable locations to alleviate groundwater stress, as agriculture accounts for 89% of water extraction in India (Suhag, 2016).

Climate change is exacerbating the frequency and duration of droughts, posing significant challenges to water supply (Dillon et al., 2019b; Hajek and Knapp, 2022; Williams and O'Gorman, 2022). MAR can help mitigate the impact of future droughts by storing rainwater. Elementary methods such as dams in Sudan (Ibrahim, 2009) or recharge wells/shafts in Bangladesh (Hossain et al., 2020) can serve this purpose. Rainwater can also be pre-treated and directly stored in aquifers using

ASR/ASTR techniques (Rinck-Pfeiffer et al., 2006), ensuring resilience in the face of water shortages (SDG 13: Climate Action). Additionally, projects in Florida have demonstrated that ASR can serve as an efficient and safe source of drinking water in highly saline aquifers (Pyne, 1995; Pyne and President, 2003). ASR can help mitigate the increasing demand for groundwater due to rising temperatures, thereby preventing over-extraction and depletion of aquifer reserves (Hossain et al., 2020; Ibrahim, 2009; Pyne, 1995). However, improperly managed ASR can lead to severe aquifer damage. Therefore, the quality of injection water should surpass that of ambient groundwater to prevent contamination (Maliva, 2020). Moreover, caution should be exercised to avoid overuse of source water for aquifer recharge to prevent environmental harm.

Pyne (1995) extensively examines the viability of ASR as an alternative water management strategy with a focus on its practicality, cost-effectiveness, and environmental compatibility. The utilization of natural underground storage in ASR renders it notably more economical than traditional surface storage reservoirs, primarily due to reduced land requirements and lower construction expenses (Maliva, 2020; Pyne, 1995). In a comparative study, it was estimated that implementing ASR for drinking water storage in the pilot project of Payson town is more cost-effective than constructing an infiltration basin with a similar volume (Lluria et al., 2018).

ASR systems contribute to enhanced efficiency in water transmission and treatment facilities, resulting in significant cost savings for utilities (Brown, 2005; Pyne, 1995). However, the successful implementation of ASR necessitates a comprehensive 2 to 3-year testing program addressing legal, environmental, and economic considerations (Pyne, 1995). ASR unit costs range from \$50 to \$160/m^3/day, with subsequent wells generally incurring lower costs (Pyne, 1995). Annual operating costs, inclusive of power, chemicals, and maintenance, range from \$1.6 to \$10.6/m^3/day (Pyne, 1995), and an alternative estimate suggests an annual operational cost ranging from approximately \$2 to \$25/m^3/day (Pyne, 2005,2014). Some of these figures date back to as early as 1995, and the actual costs today should be adjusted for inflation and other economic factors. A comparative analysis of various water storage alternatives indicates that ASR emerges as the most cost-effective option (Choi et al., 2017). Nonetheless, the cost-benefits and potential risks, such as clogging, must be carefully considered during the planning phase (Pyne, 2014).

Wendler et al. (2022) delve into the additional costs associated with treating sulphate-rich groundwaters. Groundwater sulphate concentrations exceeding 400 mg/l necessitate treatment through low-pressure reverse osmosis (LPRO) membranes, with an efficiency rate of 75–80% resulting in a 20% loss of input groundwater to concentrate flow (Wendler et al., 2022). The high energy consumption of 0.4 kWh/m^3 leads to emissions of 200 g_{CO2}/m^3 (Wendler et al., 2022), and frequent backwashing and chemical cleaning are essential for facility maintenance. The capital costs for implementing an LPRO plant are approximated at 4.1 Mio. €, including a disposal well, pipes, planning, and machinery (Wendler et al., 2022). This is however an averaged value and the actual value depends highly on the system size. To compare operational costs with ASR, a recalculation based on the production of 150,000 m^3/a (the annual volume extracted by ASR) is necessary. The proportion of overall drinking water production provided by the LPRO plant (6%; Wendler et al., 2022) is used, resulting in annual costs per unit production capacity of 164 €/m^3/d for the LPRO plant. In contrast, an ASR well, utilizing existing infrastructure with minimal adaptations, incurs construction costs of 50 €/m^3/day (\$50/m^3/day), and annual operating costs are assumed to be maximal at 10.6 €/m^3/day (\$10.6/m^3/day) due to potential improper well design (Pyne, 1995). When comparing costs, ASR using an existing well constitutes only 2% of the investment costs of LPRO, with operational expenses approximately 6% of LPRO costs. Actual costs are highly system specific, but it is clear that ASR using existing wells and recharging water that will require no further treatment can be significantly less expensive than LPRO treatment. ASR's cost-effectiveness is further emphasized by its flexibility to store surplus water in winter and meet high-demand months in summer, providing a more adaptable and cost-effective water management solution compared to LPRO.

Numerous ASR initiatives have been established with the primary aim of supplying safe drinking water to both urban metropolises (Reese, 2002) and rural communities (Murray Ricky et al., 2005). Typically, these ASR facilities are strategically sited alongside existing water treatment plants, which often operate below their maximum capacity during off-peak periods (Brown, 2005). This underutilization results in surplus water production during these low-demand intervals, creating an abundant resource for storage (Brown, 2005).

Several projects have concentrated on the retrofitting of production wells for ASR by utilizing pre-treated surface water for seasonal or emergency storage, subsequently making the recharged water available for potable use (Lluria et al., 2018; Hemenway and Grundemannz, 2002). These large-scale endeavours exhibit a remarkable capability to inject substantial volumes of water, achieving 600,000 m^3 annually in a pilot project located in Arizona, USA (Lluria et al., 2018), and successfully injecting 740,000 m^3 per year in a full-scale project situated in Colorado, USA, employing multiple ASR wells (Hemenway and Grundemannz, 2002). These endeavours have proven effective in providing drinking water to various towns across the United States, with plans in motion to expand the existing ASR capacities.

Various regions across the globe, such as central Europe, are currently undergoing significant alterations in their precipitation patterns (Williams and O'Gorman, 2022), leading to prolonged drought episodes, as exemplified by the multi-year drought spanning from 2014 to 2018 (Moravec et al., 2021). These transformations have had profound and detrimental consequences on the ecological equilibrium and operational stability of ecosystems (Dillon et al., 2019b; Moravec et al., 2021). Additionally, the ongoing process of urbanization, coupled with population expansion, has escalated the demand for potable water within metropolitan centers (Postel, 2000), all while grappling with the spatial constraints inherent in densely populated urban environments (Broere, 2016).

The aforementioned challenges are further compounded by issues pertaining to groundwater quality, originating from a variety of sources, including agricultural and mining activities (Jha et al., 2022; Sharma and Kumar, 2020; Wendler et al., 2022), as well as natural mineral dissolution processes, notably those occurring at salt domes (Posey and Kyle, 1988). Furthermore, research has underscored the heightened prevalence of surface and groundwater contamination within urban areas, surpassing that of rural counterparts, primarily attributed to industrial effluent discharges, sewage system leakages, and road salt application (Brindha and Schneider, 2019). Consequently, urban aquifers face usage restrictions due to elevated concentrations of contaminants and dissolved solids, such as chloride, nitrate, and sulphate (Brindha and Schneider, 2019; Wendler et al., 2022).

For instance, in Germany, the Hamburg metropolitan area, characterized by its high population density, confronts a significant hydrogeological challenge in the form of sulphate-rich groundwater, with concentrations reaching approximately 500 mg/l in the northwestern region. Sulphate (SO_4) is highly soluble in water, and its mobility in aquifer systems is high. Elevated sulphate levels can cause metal corrosion and health issues like dehydration and diarrhea (Sharma and Kumar, 2020). Therefore, its allowed upper threshold in drinking water in the EU is 250 mg/l (EU Directive, 2020/2184, 2021). In Hamburg, the sulphate enrichment phenomenon may potentially be attributed to the proximity of subsurface salt domes. As a consequence of stringent treatment thresholds for sulphate, several production wells have been compelled to cease operations. The constrained availability of high-quality groundwater resources has, in turn, led to a reduction in the overall production of potable water by approximately 20%. This predicament necessitates the exploration of various viable solutions, which include the construction of new wells, the incorporation of advanced Low-Pressure Reverse Osmosis (LPRO) treatment methods (Wendler

et al., 2022), or the establishment of reservoirs for drinking water storage.

In this investigation, we explore an ASR method for increasing both the storage capacity and water quality of aquifers. Our primary objective is to establish a comprehensive framework that delineates critical parameters and their associated influences when performing ASR an aquifer containing solute concentrations exceeding the prescribed drinking water quality standards with freshwater. The framework's validation is carried out through a case study centred around the metropolitan region of Hamburg, wherein certain constraints arise due to the accessibility of suitable aquifers and the substantial costs related to additional treatment processes. We examine the feasibility of repurposing abandoned production wells within aquifers characterized by elevated sulphate concentrations in a manner that is both economically efficient and ecologically sustainable. The conversion of these production wells into ASR wells is explored, along with the associated advantages of this approach.

Employing groundwater modelling software, FEFLOW (Diersch, 2014), we construct a 3D transient flow and mass transport groundwater model. This model is designed to simulate the operation of ASR on a seasonal basis within a sulphate-rich aquifer, aiming to meet the European drinking water sulphate limit. Seasonal storage involves storing water during periods of high availability and recovering it during periods of low availability (Pyne, 1995). The performance of ASR systems that store freshwater is often evaluated using recovery efficiency (RE) (Lu et al., 2011; Zech et al., 2015; Li et al., 2022). Our model serves as the baseline scenario for conducting a sensitivity analysis across a range of hydrogeological parameters, with the ultimate goal of assessing their impact on the RE.

2. Materials and methods

2.1. Governing equations

2.1.1. Groundwater flow and transport simulation

For modelling recharge cycle and the propagation of freshwater into a high solute concentration aquifer, we used FEFLOW software which describes the basic fluid flow and mass transport in porous media following mathematical equations:

Fluid flow equation:

$$S_0 \cdot \frac{\partial h}{\partial t} + \nabla \cdot \vec{q} = \sigma_f \quad \text{Eq. 1}$$

Convective mass transport equation:

$$\frac{\partial C}{\partial t} + \frac{1}{\varepsilon}\nabla \cdot (\vec{q} \cdot C) - \nabla \cdot \left(\vec{D} \cdot \nabla \mathrm{C}\right) = \sigma_m \quad \text{Eq. 2}$$

Constitutive relations:

$$\vec{q} = -\vec{k_f} \cdot \nabla h \quad \text{Eq. 3}$$

$$\vec{D} = D_m + D_d \quad \text{Eq. 4}$$

The parameter S_0 is the specific storage [1/m], h is the hydraulic head [m], $\vec{q}$ is the darcy velocity [m/s], and σ_f describes the fluidal sink/source term [g/l]. Additionally, the transport equation includes the concentration C [g/l], the effective porosity ε [−], the dynamic dispersion $\vec{D}$ coefficient [m], and the mass sink/source term σ_m [g/l]. $\vec{q}$ is proportional to the gradient of the hydraulic head ∇h. The proportionality constant is the hydraulic conductivity $\vec{k_f}$ in every defined dimension (k_x, k_y, k_z) [m/s]. The hydrodynamic dispersion D is the sum of the molecular diffusion D_m, and the hydromechanical dispersion D_d. Whereas the hydromechanical dispersion D_d is defined by the longitudinal and transversal dispersivities β_L and β_T, respectively (Diersch, 2014).

2.1.2. Numerical parameters

FEFLOW uses the finite element discretization method that although is proved to be beneficial for model performance, stability and accuracy, could have potential drawbacks, including numerical errors and numerical dispersion due to concentration front widening in discretization. To avoid these errors, we use grid Péclet number ($P_{eg} = \frac{\Delta x}{\beta_L}$) and Courant number limits (Himmel and Schäfer, 2010) to evaluate the numerical dispersion and proper discretization of the spatial grid. In the context of numerical modeling, it is imperative that grid Péclet number remains less than 2 to uphold the fidelity of the simulation. This constraint serves to maintain an accurate representation of the actual physical dispersion processes at play. When employing an explicit temporal discretization scheme, as used in this study, it is essential to ensure that the advective transport does not skip a grid cell. This requirement is encapsulated by the Courant number, which must be kept below 1 to prevent failures in the explicit numerical method. Deviating from this criterion can lead to inaccuracies and instability in the simulation (Himmel and Schäfer, 2010).

ASR performance identification.

Various quantitative methods are employed to evaluate the performance of an ASR system within a high solute concentration aquifer. In this study, we use the commonly utilized metric which is known as the recovery efficiency (RE), defined as the ratio of the recovered volume (V_{rec} [m^3]) to the injected volume (V_{inj} [m^3]) (Li et al., 2022; Ward et al., 2008, 2009; Whitehead, 1974; Zech et al., 2015):

2.2. Study area and well characteristics

The overarching goal of this study is to develop a comprehensive framework that can be applied to regions sharing hydrogeological, climatic, and anthropogenic similarities. This framework aims to systematically explore the intricate interactions between various physical parameters on RE, with a specific focus on site characteristics and operational considerations. The objective is to understand how these parameters impact the RE of ASR operations within a low-quality aquifer. This research endeavours to provide practical recommendations for ASR operators. To achieve this, a specific well site located in the northwestern area of the Hamburg metropolitan region has been chosen as a case study for groundwater modelling.

According to hydrogeological data (BUKEA, 2020), in the northwestern region of Hamburg, a seasonal variation in water extraction is observed, with an estimated monthly difference of approximately 30, 000 m^3 between summer and winter. This surplus volume is available for storage purposes and if stored in an aquifer, it can be used to meet peak water demands during dry summer months.

The study area, situated in northwestern Hamburg, is delineated as a rectangular shape, encompassing a disused groundwater abstraction well. This well ceased operation due to elevated sulphate concentrations in the groundwater. Sulphate concentrations at the well exhibit an average of about 400 mg/l, with values increasing to as high as 570 mg/l in proximity to the salt dome illustrated in Fig. 1(a). The subject well is functionally suitable for utilization from a technical perspective.

The construction materials utilized for the well and its associated screen are primarily synthetic resin-impregnated wood and polyvinyl chloride (PVC). The screen extends for a length of 40 m and partially traverses a 110-m-thick aquifer. The borehole exhibits a radius of 0.4 m.

The hydraulic heads along the eastern and western boundaries serve as suitable boundary conditions for the numerical model. The northern and southern edges are assumed to have negligible fluid exchange, as they are approximately perpendicular to the hydraulic gradient. The predominant flow direction or gradient aligns roughly parallel to the northern and southern boundaries of the model, with the western edge acting as the inflow boundary and the eastern edge as the outflow boundary.

The sensitivity of water extraction and injection from and into the

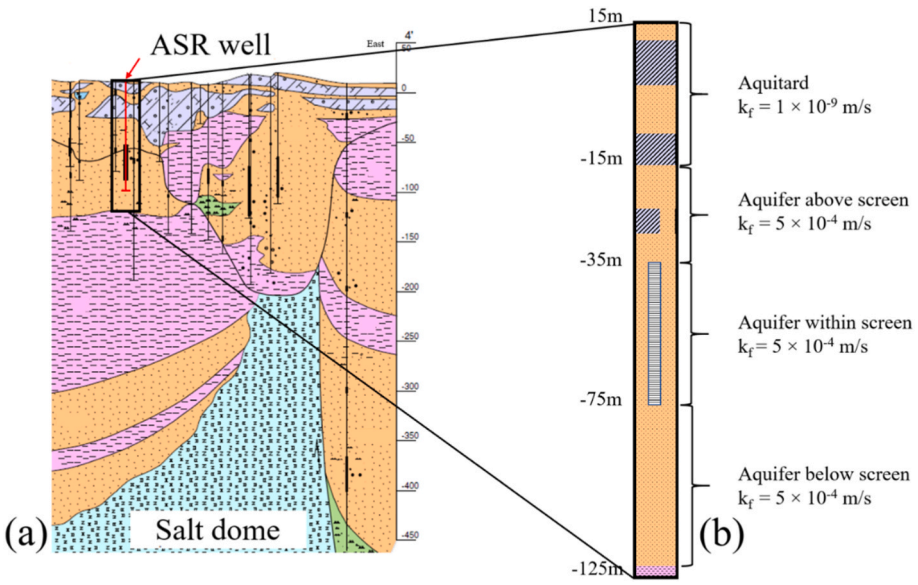

Fig. 1. Regional geological structural depiction in the proximity of the ASR well (adopted from BUKEA, 2020, a) and geological layering derived for the purposes of this study, providing a basis for analysis and interpretation (b).

abandoned well to variations across the sides of this rectangular region is later analysed to ensure that the model's spatial extent is sufficiently large to mitigate the influence of its boundaries on investigations related to ASR.

Fig. 1(a) provides a cross-sectional view of the well and the geological structure of the region. For the purposes of this investigation, we have employed a simplified representation of the geological strata, while striving to maintain a model that approximates real-world conditions. In this conceptual framework, the proposed ASR well is depicted as being partially screened within the Quaternary and Tertiary Pliocene deposits, which are primarily composed of granular materials ranging from fine to coarse sands, constituting a homogeneous aquifer. The aquifer is overlaid by the glacial till layers, discrete sand lenses, which we have collectively designated as a continuous aquitard. The hydraulic conductivity of this aquitard has been quantified at approximately 1×10^{-6} m/s based on pumping test data. In our numerical model, we have assumed the aquifer to be confined. Directly beneath the glacial till layer, there exists an aquifer with a thickness of 110 m. A hydraulic conductivity of approximately 5×10^{-4} m/s has been determined through pumping test evaluation (Manhenke et al., 2001). The base of this aquifer is sealed by the impermeable Miocene layer, composed of micaceous clay. It is vital to emphasize that the precise geological conditions are not of paramount importance in achieving the objectives of this study; rather, they serve as a foundational framework for a simplified yet realistic representation. In Fig. 1(b), we have abstracted the geological complexities and adopted a horizontal layer-based approach. The near-surface marl and sand layers, ranging from 15 m above to −15 m below sea level, have been amalgamated into a continuous aquitard. To properly model the partially penetrating well screens, we have divided the aquifer into three primary layers: the aquifer above the screen (ranging from −15 m to −35 m), the aquifer within the screen (ranging from −35 m to −75 m, with the screen spanning a length of 40 m), and the aquifer below the screen (extending from −75 m to the model's base at −125 m).

2.3. Initial and boundary conditions

To conduct a comprehensive sensitivity analysis of various parameters pertaining to the implementation of an ASR well in a sulphate-rich aquifer, we have devised a cyclic pattern for our well. Each cycle spans 365 days, designed to replicate seasonal storage dynamics. This cyclic pattern encompasses three distinct phases: an infiltration phase (typically during the rainy season) lasting 120 days, a storage period of 60 days, and an extraction phase (commonly occurring in the dry season) with a duration of up to 180 days, constrained by recovered water quality thresholds. The recovery efficiency (RE) for each cycle is computed and subsequently compared to assess parameter sensitivity and performance disparities.

To facilitate this analysis, we employ numerical modelling techniques that simulate transient fluid flow and the non-reactive, non-absorptive transport of solutes using FEFLOW 8.1 (Diersch, 2014). This approach ensures that our numerical results maintain second-order accuracy both in temporal and spatial dimensions (Diersch, 2014; Kolditz et al., 1998). The equation system solver plays a pivotal role in achieving model accuracy, stability, and performance. We employ the algebraic multigrid solver (SAMG), an iterative method well-suited for solving complex matrices associated with groundwater flow and transport equations. SAMG is known for its robustness and efficiency, leveraging multi-core computing mechanisms (Falgout, 2006). The aquifer is presumed to be confined by a glacial till layer at the bottom, rendering it impermeable. The horizontal hydraulic conductivity is determined in accordance with results obtained from pumping tests. The effective porosity is assumed to be 0.2 in fine to coarse sands (Woessner and Poeter, 2020), and the specific storage is set at 1×10^{-5} m^{-1} (Woessner and Poeter, 2020). Macro dispersivity (β_L) is crucial for model stability and the accuracy of mass transport. It serves as a modelling parameter influenced by aquifer heterogeneity. Given the inherent challenges in obtaining detailed information about porous media inhomogeneities, we employ the macro dispersivity parameter to account for unmodeled features of the aquifer (Diersch, 2014; Himmel and Schäfer, 2010). With a transport scale of approximately 100 m, the longitudinal macro dispersivity is constrained to a range of approximately 0.5 m–10 m, with smaller values between 0.5 m and 5 m being considered more reliable (Zech et al., 2015). We set the longitudinal macro dispersivity at $\beta_L = 2$ m to enable stable models with appropriate discretization. The transverse macro dispersivity is assumed to be $\beta_T = \beta_L/10 = 0.2$ m. Table 1 provides a concise summary of all pertinent material properties and model parameters, with some of these parameters varying across different scenarios.

We have defined fluid flow boundary conditions (BC) based on the predominant flow direction. The western BC is established as the inflow boundary, while the eastern BC serves as the outflow boundary. In the

Table 1
Summary of aquifer parameters.

Aquifer property	Parameter	Value	Unit
Aquifer Type	–	Confined	–
Aquifer Thickness	B	110	m
Horizontal Hydraulic Conductivity	$k_x = k_y$	5×10^{-4}	$m\,s^{-1}$
Vertical Horizontal Conductivity	$k_z = k_x/10$	5×10^{-5}	$m\,s^{-1}$
Effective Porosity	ε	0.2	–
Specific Storage	S_0	1×10^{-5}	m^{-1}
Molecular Diffusion	D_m	1×10^{-9}	$m^2\,s^{-1}$
Long. Dispersivity	β_L	2	m
Transv. Dispersivity	β_T	0.2	m

baseline scenario, we neglect the background gradient, and hence, both hydraulic head boundary conditions (1st order) are set at 11 m. On the inflow boundary, a fixed mass concentration boundary condition (1st order) is applied to the ambient groundwater, with a concentration of 400 mg/l. No mass boundary condition is necessary at the model's outflow border. To account for the ASR well, we define a well boundary condition (4th order) that includes an additional mass concentration boundary condition (1st order). Both ASR boundary conditions are regulated by a time series power function in FEFLOW, which characterizes the cyclic behaviour of the ASR well. The detailed boundary conditions are summarized along with the initial conditions for flow (hydraulic heads) and mass transport (mass concentration) in Table S3 of the supplementary materials.

The ASR well under consideration is a man-made production well. It should be noted that the construction of this well is not specifically optimized for ASR applications. The well incorporates a screen that is 40 m in length and partially penetrates an aquifer that is 110 m thick, situated between depths of −35 and −75 m below sea level. In order to facilitate ASR operations, the ASR screen is implemented as Well-BC, which is connected with a one-dimensional (1D) discrete feature element. Well-BC is positioned at the lowermost node to reconstruct a multi-layer well (MLW). This configuration offers enhanced flexibility, particularly when interfacing with Python.

The discrete feature design follows the Hagen-Poiseuille approach. It is important to note that, in compliance with the FEFLOW software's specifications, the hydraulic aperture parameter requires correction. For scenarios involving axisymmetric shapes, the hydraulic radius (r_{hyd}) and the corrected hydraulic aperture (b_{corr}) are defined as per the guidelines outlined in FEFLOW White Papers Vol. 1, 2009. Details of these equations are presented in the appendix (equations A1-A4). With a borehole radius of $R = 0.4\,m$ and constant properties of water, the hydraulic radius becomes $r_{hyd} = 0.2\,m$, and the corrected hydraulic aperture is $b_{corr} \cong 0.49\,m$. These parameters have to be set in the discrete feature element in FEFLOW.

We employed the mixed convection ratio (Ward et al., 2007, 2009), to assess the requirement for incorporating density-dependent flow. The analysis concluded that such inclusion was deemed unnecessary, given the negligible differences observed between the densities of ambient groundwater and the injected water.

2.4. Mesh generation and discretization

Mesh quality is contingent upon two critical factors: (1) the geometric integrity of the mesh and (2) the dimension of the mesh elements (Diersch in 2014). In the context of modeling ASR, the mass concentration and its gradient surrounding the ASR well assume significant roles. As freshwater infiltrates the contaminated aquifer, a pronounced concentration gradient manifests in the vicinity of the infiltration well. Consequently, it is imperative to appropriately configure the element size in the immediate vicinity of the well to ensure the attainment of precise and reliable results.

This concentration gradient diminishes as the distance from the well increases, allowing for a coarser mesh to be employed. The transition from fine to coarse mesh must be executed with care to prevent numerical inaccuracies. Specifically, the volume of the freshwater plume (V_{inj}) needs to be divided by the effective porosity (ε) to ensure that it aligns with the available open pore space within the porous media (see appendix equations A5-A6). With an infiltration volume of $V_{inj} = 150{,}000\,m^3$, an effective porosity of $\varepsilon = 0.2$ and a screen height of $H = 40\,m$, the radius would be $r \cong 77\,m$. For the distance around the well, $\sim 100\,m$ is used as a rough estimation. The first model tests underline the approximation to be true. Therefore, this distance can be used to approximate the mass transport length.

To generate the mesh, a polygon delineating the geographical area under investigation, along with a georeferenced point representing the ASR well, were employed. The study area polygon was subdivided to create a rectangular region encompassing the ASR well location, with each side measuring approximately 200 m. Within this specific vicinity surrounding the well, a finer discretization was established. To leverage these elements for mesh refinement, a high-speed and robust 2D triangulation tool known as "TRIANGLE" was employed to generate the mesh. This triangulation process yields high-quality triangular meshes suitable for various scientific applications (Diersch, 2014, p. 770). The 3D layer configurator was subsequently utilized to extend the 2D mesh into a 3D layered mesh. The vertical discretization of the model domain, which was attained through the utilization of the geological structure depicted in Fig. 1 was accomplished by assuming the presence of horizontally stratified layers and employing vertical mesh refinement to achieve the desired level of discretization. Taking into account the maximum allowed Péclet and Courant numbers, the geometric configuration encompassing the well exhibits an average element diameter of 1.85 m, while the vertical discretization of the aquifer was established at 2 m. These parameters underwent validation through a numerical stability analysis. In order to circumvent Courant criterion violation, the maximum time step size was established at 2 days, while the critical time step size (Δt_{crit}), was estimated to be 0.1 day. A maximum time step size of 0.1 day was implemented during the initial model cycle to mitigate numerical dispersion.

2.5. Model dimensions

The dimensional parameters of the model hold a significant sway over its precision and efficacy. Striking a balance is crucial: the model's boundaries must reside at a considerable distance from the well to mitigate boundary effects on the model's results, yet computational efficiency remains a pivotal consideration. In a concise simulation spanning 90 days; comprising 30 days each for infiltration, storage, and extraction; two models underwent scrutiny to ascertain the impact of both model size and the proximity of the ASR well to the model's boundary conditions. These models, embodying an identical conceptual framework and sharing a similar discretization, explored two scenarios: ASR application exclusively and ASR application coupled with a production well. The smaller model featured dimensions of 1000 m × 2000 m, while its counterpart doubled in size at 2000 m × 4000 m. The investigation focused on hydraulic heads and mass concentration distribution, delving into the effects of boundary conditions to determine an optimal model size. To ensure uniformity, horizontal mesh generation was deployed in distinct regions of the model area, maintaining consistency around the well in both the "small" and "large" models. Within these designated regions, an equivalent number and distribution of elements were established in both models, fostering a comprehensive comparative analysis. Our analysis revealed that the variation in simulated hydraulic heads within corresponding areas of both models remains within a margin of 1.5%, with a notably lower discrepancy observed in the vicinity of the ASR-Well (≤0.5%). The disparities in mass distribution imply that the error predominantly falls within the range of 2%, although certain discrepancies in the vicinity of the ASR well surpass 4%. These inconspicuous errors lack discernible patterns

and are anticipated to arise from subtle variations in discretization, both temporally and spatially. Upon scrutinizing the cumulative extracted mass of both models, it is evident that the overall disparity is less than 0.02%. Consequently, the identified discrepancies likely stem from numerical discretization errors, offsetting one another in aggregate. Hence, these errors may be deemed negligible, affirming the suitability of the "small" model for the intended modeling objective.

2.6. Operational scheme

In this study, we aim to compare and evaluate the local flow dynamics over multiple cycles. The metric employed for this assessment is the recovery efficiency (RE), recognized as the most pertinent parameter to gauge the operational viability (Ward et al., 2008). Notably, RE serves as a comprehensive integrator, enabling an overarching analysis of entire flow systems without delving into intricate flow and transport details. To establish a practical threshold for freshwater concentrations in compromised aquifers, we adopt the European drinking water standard for sulphate (C_{limit} = 250 mg/l, EU Directive, 2020/2184, 2021).

The ASR process unfolds through a cycle of injection, storage, and extraction (see Figure A1 in Appendix) adhering to the schematic cycle definition employed in this investigation. The blue line signifies the pumping rate (negative for infiltration and positive for extraction), while the orange line outlines a schematic concentration curve. Dotted lines denote fixed values defined within the model.

Commencing with a 120-day injection phase, ambient groundwater with elevated concentrations (C_{amb}) is displaced by the injected freshwater (C_{inj}). The subsequent storage duration spans 60 days. During the extraction phase, water is pumped from the aquifer, resulting in concentration increase at the well. Extraction automatically halts when the predefined concentration limit (C_{limit}) is reached. For the remainder of the year (up to 365 days), the well remains inactive. While conventional studies often equate extraction and injection times, this temporal constraint becomes a limiting factor for extraction before reaching the concentration threshold. Consequently, the recovery efficiency (RE) is capped at 100% (RE $\leq$ 100%). To introduce flexibility and explore long-term possibilities of ASR, the time limit is extended to 180 days, yielding RE $\leq$ 150%. This adjustment ensures that the maximum extraction time no longer imposes a restrictive factor on recovery efficiency. Therefore, in our study, The RE is defined as:

$$RE = \frac{V_{rec}}{V_{inj}} = \frac{Q_{rec} \cdot (t_3(C = C_{limit}) - t_2)}{Q_{inf} \cdot (t_1 - t_0)} \leq 150\ \% \qquad \text{Eq. 5}$$

The total RE is additionally evaluated as overall efficiency. In an ideal case, when the injection time is always the same, the total RE equals the mean RE. Care must be exercised in instances involving the target volume storage (TSV) approach—an approach designed to store water for the establishment of a buffer zone around the well prior to the commencement of cycle testing. Here, where the initially injected volume has to be considered and the total RE is defined as:

$$RE_{tot} = \frac{\sum_{n=1}^{5} V_{rec,n}}{\sum_{n=1}^{5} V_{inf,n}} \qquad \text{Eq. 6}$$

2.7. Initial and boundary conditions: scenarios

Each scenario presented adheres to the foundational baseline scenario outlined earlier. To yield meaningful and discerning results, the scenarios must span a broad spectrum of multiple parameters within a judicious scale, allowing for the measurement of sensitivity to variations in each parameter. Selection of parameters for transport modelling aligns with established literature (Pyne, 1995; Antoniou et al., 2017; Woessner and Poeter, 2020) and is catalogued in Table 2.

Incorporating diverse scenarios requires specific configurations, as outlined below.

Table 2
An overview of parameter values corresponding to each scenario, with bolded values denoting the baseline scenario for reference.

Scenario	Parameter	Value	Unit
Gradient	$\boldsymbol{I} = \frac{\Delta h}{l}$	$\mathbf{0}, 0.5, 1, 2.5$	‰
Gradient (Flow)	$q = \boldsymbol{k_f} \cdot \boldsymbol{I}$	$k_f = 1{\cdot}10^{-4}\ m/s;\ I = 2.5‰$	
Hydr. Conductivity	$\boldsymbol{k_x}, k_x = k_y, k_z = \frac{k_x}{10}$	$1{\cdot}10^{-5}, \mathbf{5{\cdot}10^{-4}}, 1{\cdot}10^{-3}$	m/s
Heterogeneity	$\boldsymbol{k_x}, k_x = k_y, k_z = \frac{k_x}{10}$	$5{\cdot}10^{-5}, 1{\cdot}10^{-4}, \mathbf{5{\cdot}10^{-4}}$	m/s
Dispersivity	$\boldsymbol{\beta_L}, \beta_T = \frac{\beta_L}{10}$	$1, \mathbf{2}, 5, 10$	m
Aquifer Type	–	**Confined**/Unconfined	–
Aquifer Thickness	$\boldsymbol{B}$	$60, \mathbf{110}, 160$	m
Effective Porosity	$\boldsymbol{\varepsilon}$	$0.05, 0.1, \mathbf{0.2}, 0.3$	–
Specific Storage	$\boldsymbol{S_0}$	$\mathbf{1{\cdot}10^{-5}}, 5{\cdot}10^{-5}, 1{\cdot}10^{-4}, 1{\cdot}10^{-3}$	1/m
GW Concentration	$\boldsymbol{C_{amb}}$	$\mathbf{400}, 600, 800, 1200, 1600$	mg/l
FW Concentration	$\boldsymbol{C_{inj}}$	$100, \mathbf{150}, 200$	mg/l
Pump Rate	$\boldsymbol{Q_{inj}} = \boldsymbol{Q_{rec}}$	$25, \mathbf{50}, 100, 150$	m^3/h
Operation Mode	Previous **TSV** Injection	$\mathbf{0}, 144000$	m^3
Operation Mode	**TSV** and $\boldsymbol{C_{amb}}$	$C_{amb} = 800\ mg/l;\ TSV = 144000$	
Second Well	Second Well (Distance)	$400, 200, \boldsymbol{No}$	m

2.7.1. Modelling heterogeneity

Hydraulic conductivity heterogeneity was delineated within a 20 m thick layer at the centre of the well screen. This layer exhibited a hydraulic conductivity distinct from that of the surrounding aquifer. The aquifer is characterized by a sand layer, while the marl layer serves as the confining layer. A transitional layer, introduced for model stability considerations, separates the aquifer from the aquitard. The heterogeneity layer comprises slices with varied hydraulic conductivity values.

2.7.2. Modelling operation mode (TSV)

The TSV approach underwent testing with consistent parameters, encompassing a maximum extraction duration of 180 days and concentration limits. While these settings may not align with real-world applications, they facilitate a comparative analysis against the baseline scenario. Preceding the initial ASR cycle, a TSV cycle involved injecting TSV without subsequent extraction. To comprehensively assess the TSV approach's impact, scenario replication ensued with an ambient concentration of 800 mg/l and a maximum extraction duration of 132 days, yielding a maximum Recovery Efficiency (RE) of 110%. This nuanced evaluation offers a comprehensive understanding of the effects.

2.7.3. Modelling hydraulic gradient

To induce a hydraulic gradient in the model, the East BC was configured with a lower hydraulic head. This adjustment resulted in an overall gradient (I = Δh/l), considering a model length (l) of 2000 m. Furthermore, the maximum gradient scenario (I = 2.5‰) was coupled with a moderate hydraulic conductivity ($k_f = 1 \times 10^{-4}$ m/s) to scrutinize the combined effects of these two hydraulic properties.

3. Results

3.1. Baseline model

Fig. 2 presents the mass concentration distribution at various temporal points during both the injection and extraction phases of the first cycle through a vertical cross-section. The simulation initiates from the initial condition, wherein the ambient groundwater concentration (C_{amb}) is set at 400 mg/l. Following 10 days of injection, a diminutive injection water plume displaces the ambient groundwater surrounding

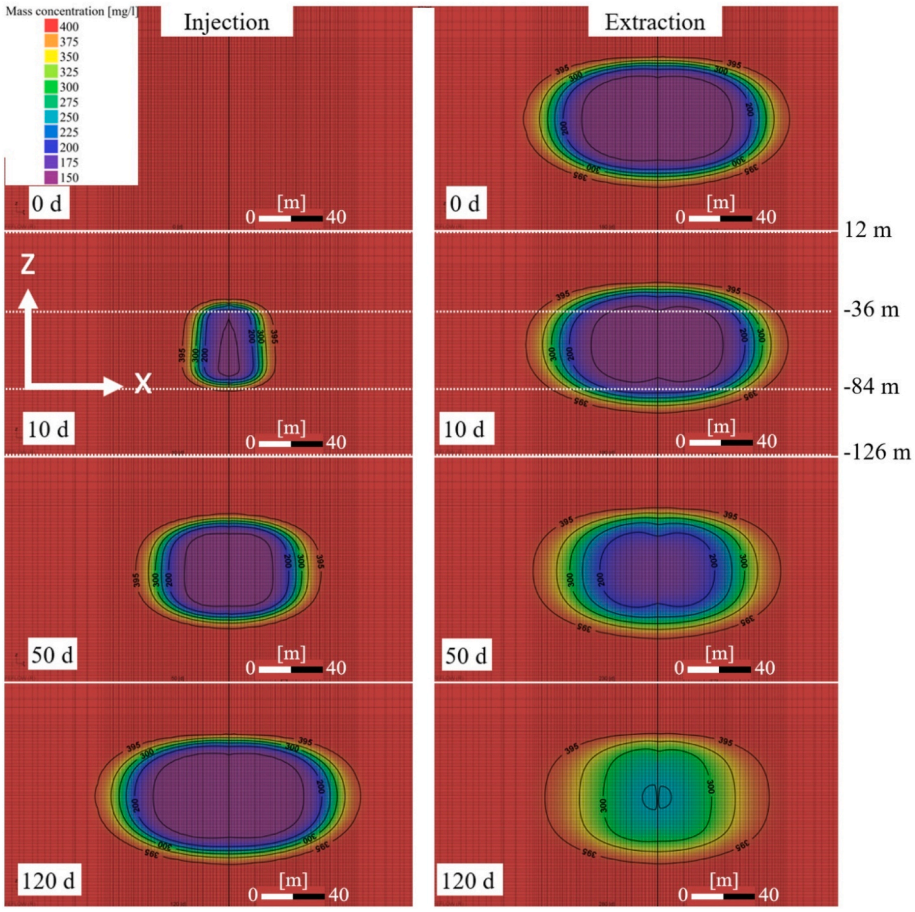

Fig. 2. Baseline scenario depicting the temporal process of mass propagation during the injection and extraction phases of the first cycle through a vertical cross-section.

the well, revealing a pronounced concentration gradient at the mixing zone between the injected and ambient water.

As injection progresses, the plume expands, and the transition zone undergoes widening. Notably, during the storage phase occurring between injection and extraction (spanning 60 days), no observable effects are manifested. The extraction phase illustrates a diminishing plume after 10 days. Over subsequent extraction periods, the plume continues to decrease, accompanied by a concurrent flattening of the concentration gradient. Upon reaching the conclusion of the extraction process (approximately 100 days), the concentration at the well surpasses the designated limit of 250 mg/l, prompting the cessation of extraction. In the vicinity of the well, a broad transition zone persists, demarcating the well from the ambient groundwater. Notably, the expansion of this transition zone is distinctly evident in comparison to its state at the initiation of the injection period (10 days).

Fig. 3 presents a representative excerpt from the numerical model output, illustrating the impact of concentration-limited extraction across multiple cycles. The concentration profiles initiate at the ambient concentration of 400 mg/l, rapidly decreasing to the injected concentration at the commencement of injection. Throughout the storage phase, the concentration remains constant at the well due to the absence of lateral flow in the baseline model. Upon entering the recovery phase, the concentration increases until reaching the predefined concentration limit. Subsequently, the pump ceases operation, and the concentration remains steady for the remainder of the cycle. As the number of cycles increases, the breakthrough curves during recovery exhibit a

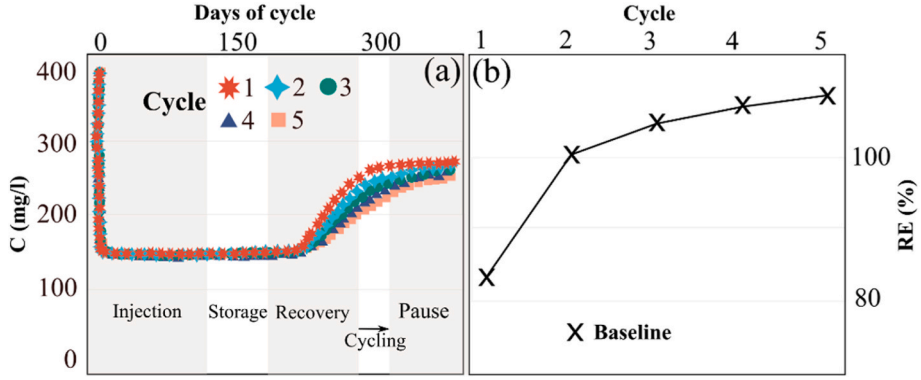

Fig. 3. Temporal evolution of mass concentration (C; a) and recovery efficiency (RE) across five cycles of the baseline scenario (b).

diminishing slope, leading to an extended extraction time. In our investigation, the breakthrough curves pertaining to sulphate concentrations during the extraction process stand out as a focal point of interest.

During the first cycle, the extraction rapidly attains the concentration limit (RE = 81%), resulting in 19% of the infiltrated volume persisting within the aquifer and contributing to the dilution of ambient groundwater surrounding the well. Subsequently, in the second cycle, the concentration of the mixed water in the vicinity is recorded as ≥250 mg/l, as opposed to the initial 400 mg/l, with further dilution occurring through the infiltrated water. The extraction phase reveals the dilution effect through a discernible reduction in the slope of the breakthrough curve. This behaviour is particularly pronounced in the initial two cycles and gradually diminishes until a quasi-steady state is achieved. To streamline the presentation of pivotal insights, we showcase the 1st and 5th cycles of each scenario set, complemented by a RE-Plot depicting RE dynamics across the cycle continuum in Fig. 3(b). This figure illustrates the efficiency progress across multiple cycles. The initial state, denoted as the baseline scenario, commences with an efficiency (RE) of 81%, demonstrating an ascending trend throughout subsequent cycles, ultimately peaking at RE_5 = 110%. The efficiency curve exhibits a gradual plateauing effect as cycles advance, approaching quasi-steady state conditions around the fifth cycle.

3.2. Scenarios

Fig. 4 serves as visual representations of the sensitivity analysis scenarios, specifically focusing on the outcomes associated with the 1st and the 5th cycle RE. This sensitivity analysis reveals that the RE of the 1st cycle is predominantly influenced by factors such as the hydraulic gradient (I), ambient concentration (C_{amb}), injection concentration (C_{inj}), and dispersivity (β_L, β_T). Notably, these parameters exhibit a high degree of sensitivity. Conversely, the effective porosity and pumping rate demonstrate a moderate level of sensitivity concerning RE. On the other hand, parameters like heterogeneity, hydraulic conductivity, specific storage, and aquifer type do not exhibit significant sensitivity within the scope of this study. A comprehensive summary of the results obtained from scenario simulations is provided in Table S2 in the supplementary materials.

Throughout the five cycles examined, the baseline scenario demonstrated an increase in RE, rising from 81% to 110%. With the exception of the hydraulic gradient scenario, efficiency exhibited improvement with an increasing number of cycles, as illustrated in Fig. 4(a). Notably, the parameter with the lowest RE in a given scenario during the 1st cycle underwent the most substantial enhancement, and conversely, leading to a convergence of parameters within each scenario set as the cycles progressed. Noteworthy is the reversal of the pump rate scenario's order between the 1st and 5th cycle. The RE of the 5th cycle demonstrated heightened sensitivity to the hydraulic gradient (I), ambient concentration (C_{amb}), injection concentration (C_{inj}), and dispersivity (β_L, β_T). Conversely, the effective porosity, aquifer thickness, aquifer type, specific storage, hydraulic conductivity, and pump rate exhibited negligible sensitivity to the efficiency of long-term ASR operation.

In the following, an in-depth analysis is conducted on scenarios involving the parameters exhibiting the highest sensitivity as well as a discussion over the parameters demonstrating lower sensitivity is undertaken.

3.2.1. Hydraulic gradient

The background hydraulic gradient exerted a noteworthy influence on the recoverable volume. The intricate interplay of mass concentration distribution and transport processes is elucidated in greater detail in Fig. 5 for hydraulic gradients of I = 0.5 ‰, I = 1.0 ‰, and I = 2.5 ‰, respectively. This figure, which is the top view of a horizontal cross-section at z = −55 m, illustrates a discernible shift in the injection plume during every phase of the cycle, with the plume assuming an elliptical shape during injection. These effects become increasingly pronounced with steeper hydraulic gradients. While the deformation during injection remains negligible for a low gradient of 0.5 ‰, it becomes more severe for a gradient of 2.5 ‰.

A parallel observation can be drawn when examining the freshwater movement until the conclusion of the storage phase. In the case of a low gradient (0.5 ‰), the well remains within the confines of the pure injected water. Conversely, for a substantial gradient (2.5 ‰), the well resides in the transition zone at a concentration of approximately 300 mg/l. This phenomenon is further illustrated in Fig. 6(a).

Fig. 6(a_3) underscores the impact of the gradient on the RE. A modest gradient of 0.5 ‰ results in a substantial reduction in efficiency (1st cycle ~20%, 5th cycle ~46%) compared to the baseline scenario devoid of a gradient. Furthermore, there is a lack of efficiency improvement with successive cycling, except for a marginal increase of ~3% in the variant with the lowest gradient (0.5 ‰).

3.2.2. Ambient concentration

Fig. 6(b) illustrates the breakthrough curves of mass concentration during the 1st and 5th cycles under various ambient concentrations. Notably, elevated ambient concentrations correspond to increased gradients and steeper breakthrough curves. This trend persists in the 5th cycle. Nevertheless, the slopes of the curves exhibit a notable reduction, accompanied by an extension in the extraction duration.

Consequently, there is a discernible augmentation in RE across cycles, as evident in Fig. 6(b_3). It is noteworthy that the relative differences between the parameters persist in the long-term analysis.

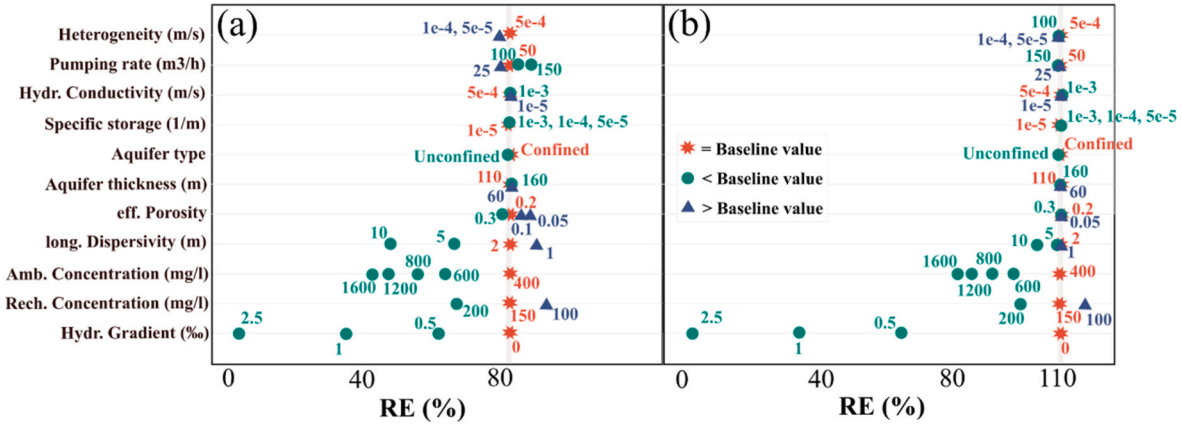

Fig. 4. Overview of the sensitivity analysis scenarios results for the (a) 1st and (b) 5th cycle recovery efficiency (RE).

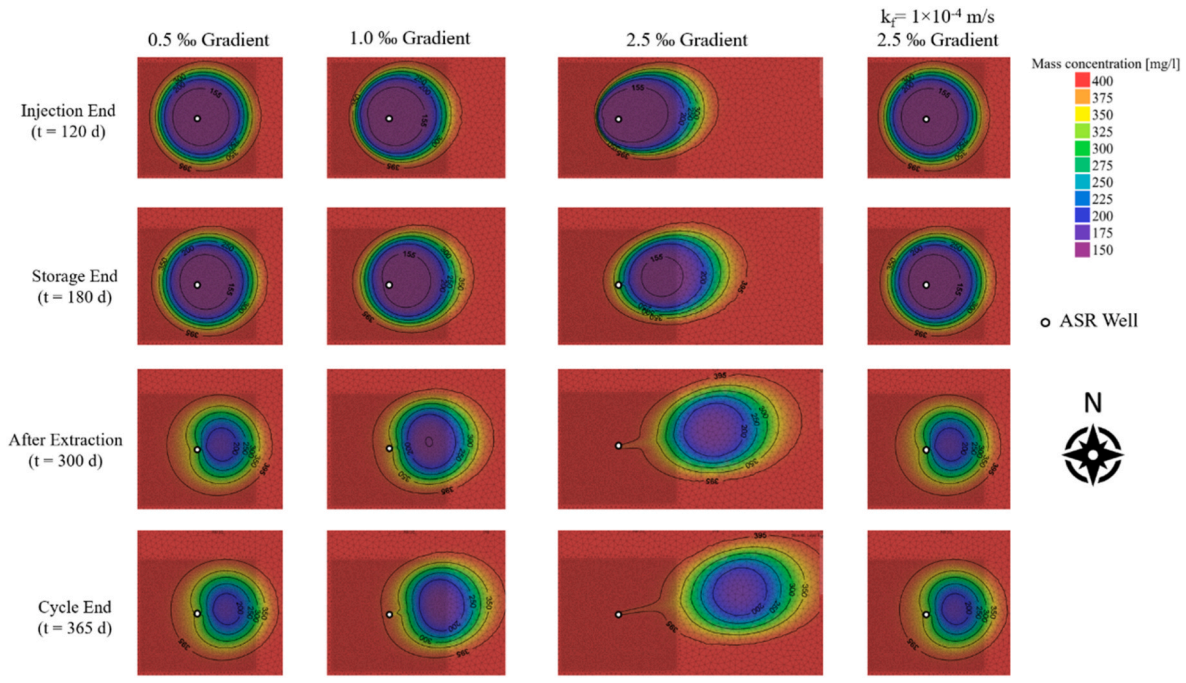

Fig. 5. Top overview of a horizontal cross-section at z = −55 m, showing mass propagation during the first cycle under varying hydraulic gradients. The influence of hydraulic conductivity is depicted as the hydraulic gradient undergoes fluctuations, as further elaborated in the discussion section.

3.2.3. *Injection concentration*

Variations in the freshwater concentration exhibit a discernible impact on the breakthrough curves, as elucidated in Fig. 6(c). The intersection of the transition zone coincides across all scenarios, yet lower injection concentrations manifest a more rapid escalation, characterized by pronounced concentration gradients. In the 5th cycle, the gradients undergo a discernible attenuation while maintaining distinct profiles, resulting in disparate extraction durations. This phenomenon is further corroborated by the RE plot in Fig. 6(c_3), demonstrating a consistent efficiency gap throughout the cycles. Notably, the optimal RE of 117% is attained at a low injection concentration of 100 mg/l. Nevertheless, a higher concentration of 200 mg/l, proximal to the limit concentration, exhibits commendable performance with a RE of 98%.

3.2.4. *Dispersivity*

Fig. 6(d) depicts the breakthrough curves during the 1st and 5th cycles for the dispersivity scenario, showcasing the extraction process. Commencing at an injection concentration (C_{inj}) of 150 mg/l, the extraction culminates at the defined limited concentration (C_{limit}) of 250 mg/l for each dispersivity value, albeit with distinct progressions. Notably, the breakthrough curve for the highest dispersivity of 10 m exhibits an immediate and nearly constant slope until it attains the limit concentration. Subsequently, other curves, representing varying dispersivity values, ascend with varying delays, following a sequence from large to small dispersivity values. Additionally, the breakthrough curves transition from linear to curved trajectories.

It is noteworthy that with decreasing dispersivity, there is a noteworthy extension in the duration of the extraction process. Upon examination of the breakthrough curves during the 5th cycle, the overall shape of the curves remains consistent, yet the endpoints converge. This convergence phenomenon is further illustrated in the RE plot depicted in Fig. 6(d_3).

3.2.5. *Effective porosity*

Fig. 6(e) depicts the breakthrough curves during the 1st and 5th cycles within the context of the effective porosity scenario. The concentration profiles exhibit a consistent progression, albeit with a subtle horizontal displacement.

Notably, the curves associated with the lowest porosity are positioned to the right, while those linked to the highest porosity are situated to the left. In the subsequent 5th cycle, the breakthrough curves exhibit a slight flattening, converging to a common endpoint. It is noteworthy, however, that despite their shared final position, these curves traverse distinct trajectories. Commencing uniformly, the curves diverge during their ascent and subsequently reconverge at the culmination. In fact, our results have shown that, smaller porosity values correspond to an augmented spreading of the infiltrated bubble, thereby yielding a broader transition zone. This phenomenon is indicative of increased dispersion. Notably, during the 1st cycle, a substantial volume of injected water persists within the storage zone, underscoring the impact of porosity on water retention dynamics.

3.2.6. *Pumping rate*

With escalating pumping rates, the volumes infiltrated (and subsequently extracted) experience augmentation, while the recharge duration remains constant. Fig. 6(f) depict the breakthrough curves for the 1st and 5th cycles, respectively. Minimal variations manifest in the 1st cycle, diminishing further throughout subsequent cycles. The RE behaviour mirrors this trend. In the 1st cycle, curves exhibit similar but marginal deviations. Lower pumping rates correlate with an early ascent, while higher rates correspond to a delayed ascent, resulting in higher RE values for increased pumping rates and vice versa. However, during the 5th cycle, the RE remains consistent across all pump rates. A comparative analysis between the 1st and 5th cycles reveals a substantial expansion of the transition zone in the latter. This observation holds true when comparing equivalent cycles at different pump rates, where higher pump rates lead to an enlarged buffer zone. This phenomenon persists in both the 1st and 5th cycles.

In addition to the sensitivity analysis of parameter scenarios, we investigated the impact of two specific operational strategies on RE: target volume storage (TSV), which entails the storage of water to establish a buffer zone around the well before initiating cycle testing; and the placement of a neighbouring production well in proximity to the ASR well.

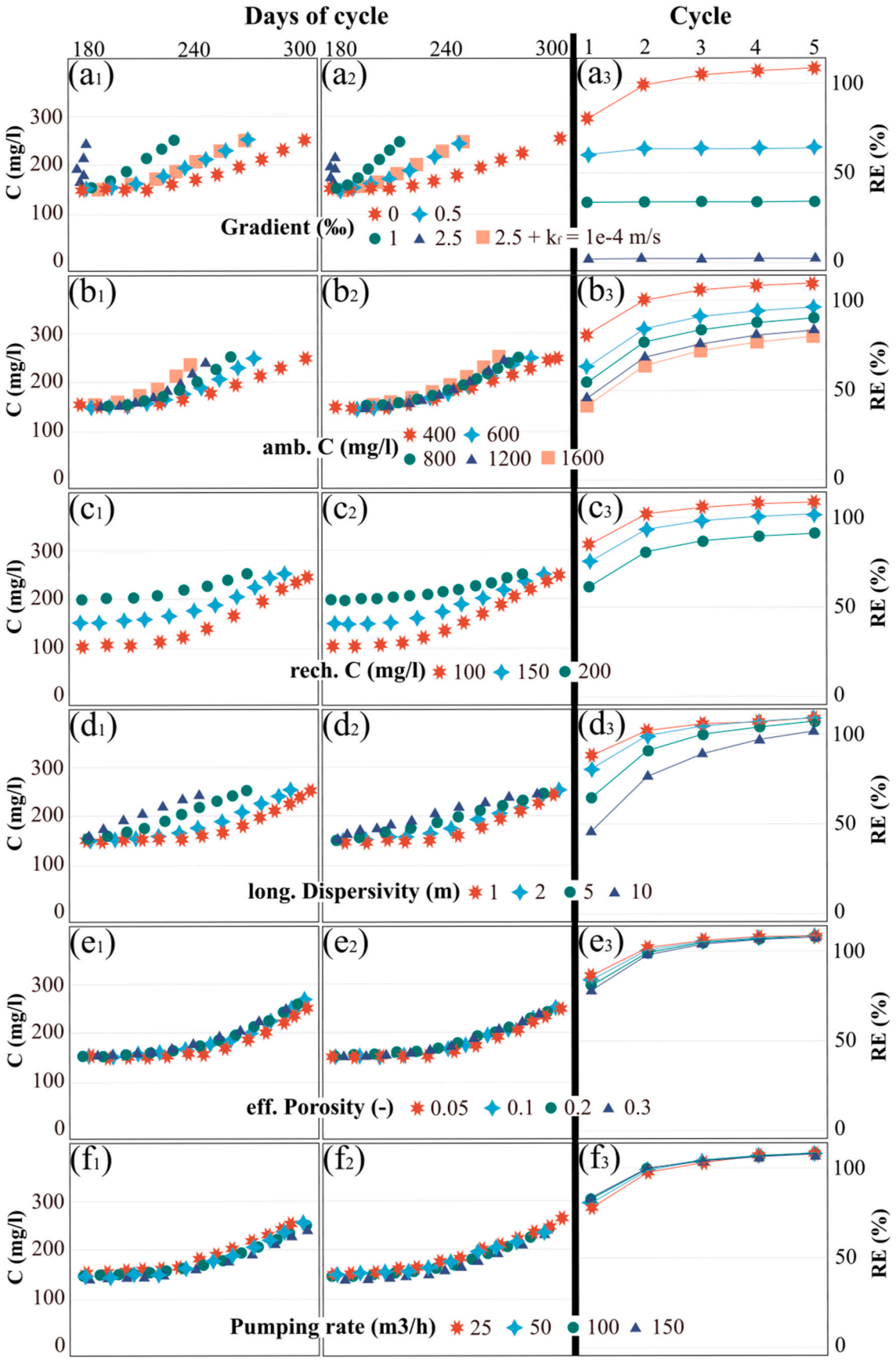

Fig. 6. Breakthrough curves of mass propagation (C) under varying hydraulic gradients (a), ambient concentrations (b), injection (recharge) concentrations (c), dispersivities (d), effective porosities (e), and pumping rates (f) during the first (X_1) and fifth (X_2) cycles as well as the progression of recovery efficiency (RE) through cycles (X_3).

3.2.7. TSV operation mode

Fig. 7(a) depicts the mass concentration distribution for the operation mode employing a TSV scenario. The four temporal steps encompass contributions from the initially injected TSV before commencing ASR cycling, as well as during the subsequent recharge and recovery phases (300 days and 365 days) of the first cycle. Preceding the cycling phase, the TSV is introduced into the storage zone surrounding the ASR well, and the injection stage of the first cycle further augments the water content within the storage. Notably, in comparison to the baseline scenario, the total injected water is twofold. Consequently, the recovery during the first cycle attains the maximum defined extraction volume of 150%, and residual water persists around the ASR well, satisfying extraction conditions. However, it is imperative to acknowledge that this RE does not consider the TSV injected before.

Fig. 7(b) presents a comparison between the RE plot of the TSV approach and the baseline scenario. The RE curve for the TSV approach initiates at the maximum defined efficiency of 150% and gradually converges to the quasi-steady state condition of the baseline scenario, reaching REs of approximately 112%. Moreover, breakthrough curves for the 5th cycle in Fig. 7(c) exhibit a sustained long-term similarity. The RE incorporates the TSV injected, resulting in an unbiased estimation. The total RE for the TSV approach is projected to be 100.7%, aligning it with the baseline scenario.

3.2.8. Neighbouring production well

In two distinct scenarios, we positioned the production well at distances of 200 m and 400 m from the ASR well. Fig. 8, which is the top view of a horizontal cross-section at z = −55 m, delineates the mass concentration distribution across various scenario variants with a proximate production well. The left panel illustrates concentration dynamics for a neighbouring well situated 200 m away, while the right panel depicts concentrations at a 400 m distance. Throughout successive phases, the isolines of mass concentration progressively curve towards the production well. This phenomenon is accentuated over time and as the distance to the production well decreases. However, this influence is confined to the mass located on the west side (in the direction of the production well) of the ASR well, leaving other cardinal directions unaffected. At the conclusion of the first cycle, the isolines on the left side (200 m) exhibit an egg-shaped configuration, whereas those on the right side (400 m) display only slight deformation.

The closer production well (at 200 m) initiates with an efficiency of approximately 75%, escalating to 86% in the second cycle. Nonetheless, while the RE for the other scenarios (baseline and 400 m) continues to increase with subsequent cycles, the 200 m variant reaches its efficiency zenith at 88%, followed by the 400 m scenario, which attains a limited long-term efficiency of approximately 102%.

4. Discussion

We delved into an innovative strategy for addressing contemporary water supply challenges arising from urbanization, climate change, and concerns related to groundwater quality. The investigation centers on

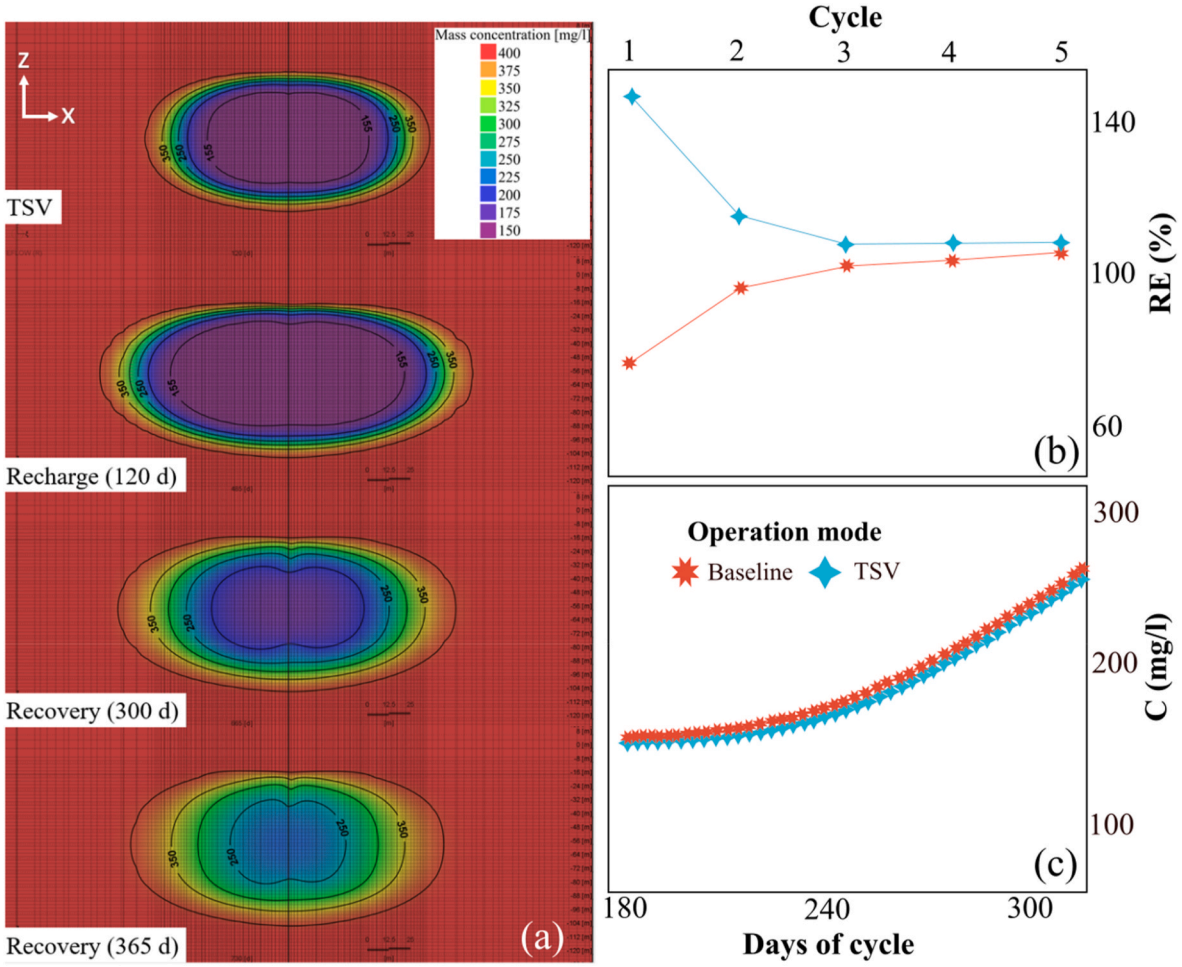

Fig. 7. Mass transport dynamics in the operation mode scenario featuring target volume storage (TSV) displayed for a vertical cross-section along the well in the first cycle (a); comparative Analysis of Recovery Efficiency (RE) between the Baseline scenario and the target volume storage (TSV) Operation Mode (b) and breakthrough curves depicting mass propagation (C) in the fifth cycle for both scenarios (c).

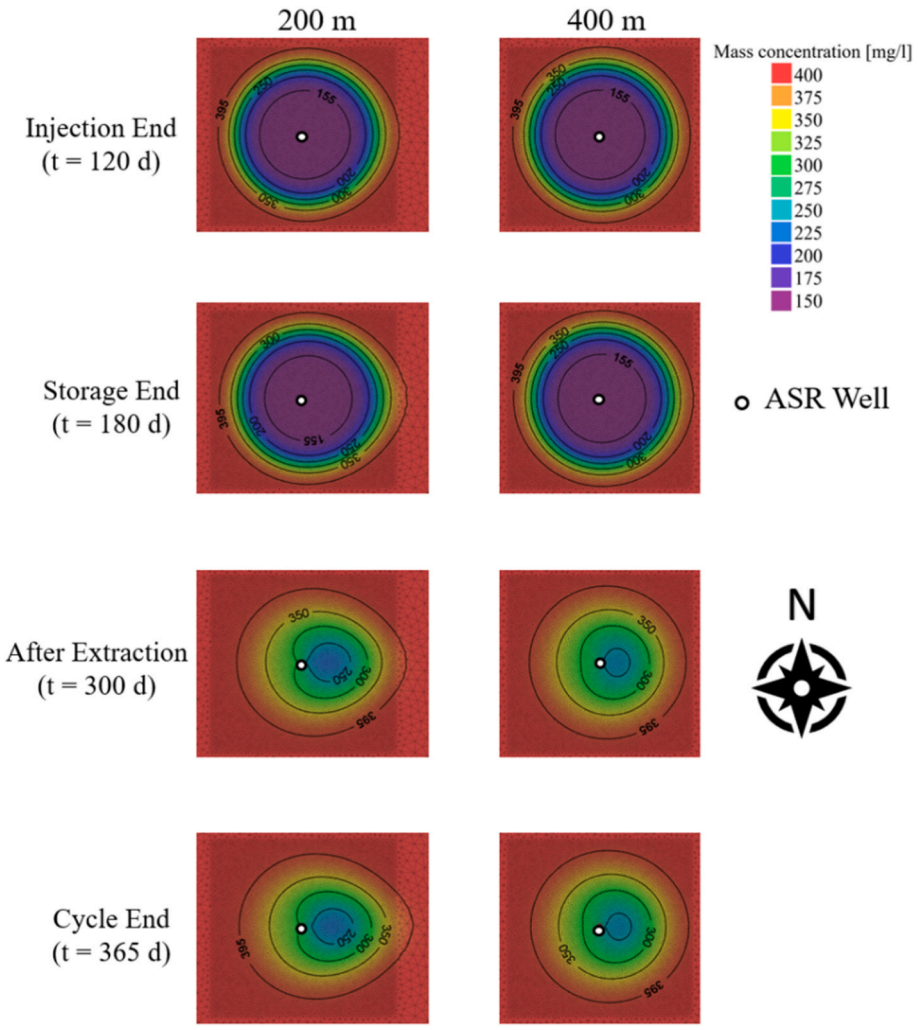

Fig. 8. Top overview of the horizontal cross-section at z = −55 m depicting mass propagation in scenarios of neighbouring production wells positioned at distances of 200 m and 400 m to the right of the Aquifer Storage and Recovery (ASR) well.

the feasibility of repurposing production wells for ASR operations within saline aquifers, with a specific emphasis on well construction considerations. Utilizing a groundwater flow and transport model, the study assesses the influence of site-specific hydrogeological factors and operational parameters on Recovery Efficiency (RE). The comprehensive analysis also incorporates economic dimension to afford a holistic understanding of ASR. The results reveal a general increase in RE with successive cycles, although exceptions are noted for the hydraulic gradient, where RE remains relatively constant between the 1st and 5th cycles. Notably, the hydraulic gradient, ambient and injection concentrations, and dispersivity emerge as the most influential parameters affecting efficiency. In contrast, factors such as heterogeneity, hydraulic conductivity, specific storage, and aquifer type exhibit minimal impact on RE within the scope of this investigation.

Baseline scenario results reveal that cycling increases recoverable volume. This phenomenon is due to the presence of a mixture of injection and ambient water in the storage zone at the end of extraction, forming a barrier between ambient groundwater and the ASR well (see Fig. 2 at 120 days of extraction). This lowered concentration bubble allows a higher mixing fraction of transition zone water with injection water without exceeding the limit concentration of 250 mg/l. This effect augments the RE for subsequent cycles until reaching a quasi-steady state RE of approximately 112% after 10 cycles. The observed increase in RE during cycling is consistent with prior studies by Pyne (1995) and Merritt (1985, 1986) which simulated ASR scenarios with a chloride limit of 250 mg/l. This phenomenon is further supported by practical observations documented by Pyne and President (2003).

Previous modelling studies and field data on ASR in brackish or saline aquifers, as summarized by Maliva (2020) and Maliva et al. (2019), indicate an inverse relationship between system efficiency and salinity in the storage zone, a relationship found to be equally valid for lower concentrations and concentration gradients. For a baseline scenario concentration of 400 mg/l, ASR achieves REs of 110% after a few cycles, but when storage zone concentrations exceed 1600 mg/l, long-term REs decrease to below 80%. Despite this, the operation remains economically feasible, as water can be recovered during times of high demand or low supply, adding value to the process (Maliva, 2020). Fig. 6(b) compares scenarios with ambient concentrations ranging from 400 mg/l and 1600 mg/l for the 1st and 5th cycle, indicating consistent efficiency differences with cycling due to the steeper concentration gradient for higher ambient concentrations. Both ambient and injection concentrations are crucial parameters, as the maximum mixing ratio is entirely dependent on them when a fixed extraction limit is established. High concentrations (ambient or freshwater) near the limit concentration necessitate careful mixing to avoid exceeding water quality limits. The more permissible the mixing of recharge and ambient water without violating quality limits, the greater the water in the transition zone that can be recovered. These considerations underscore the significance of both concentrations as long-term parameters, as demonstrated by the influence of salinity on RE in saline aquifers with high ambient

concentrations (Maliva, 2020; Merritt, 1985, 1986).

Lateral groundwater flow, resulting from the hydraulic gradient, is pivotal for ASR efficiency, especially in highly conductive porous media. In the sensitivity analysis, the hydraulic conductivity (k_f) did not significantly affect the RE of the base model (with I = 0) within the range of 10^{-3} to 10^{-5} m/s. Similar findings are reported by Merritt (1985, 1986). In cases of a high lateral gradient (I = 2.5 ‰) and base model hydraulic conductivity, the results indicate a nearly complete loss of injected water due to groundwater flow. Conversely, lower horizontal hydraulic conductivity ($k_x = 1 \times 10^{-4}$ m/s) in the same situation results in a RE of ~60%. These findings emphasize the crucial role of flow velocity $q = k_f \times I$, where horizontal hydraulic conductivities (k_x, k_y) become significant, compensating for higher gradients. Scenarios with equal Darcy flux (I = 0.5 ‰ with $k_f = 5 \times 10^{-4}$ m/s and I = 2.5‰ with $k_f = 1 \times 10^{-4}$ m/s) result in similar mass transport behaviour, breakthrough curves, and REs. These observations align with findings from several studies summarized by Maliva (2020) and Ward et al. (2009).

Scenarios with a neighbouring production well at different distances from the ASR well (400 m and 200 m) lead to a reduction of long-term RE to 102% and 88%, respectively. This decline in RE is attributed to the hydraulic gradient induced by pumping from the production well. In contrast to the background hydraulic gradient, the flux caused by the production well varies in the storage zone from 7.6 mm/d to 16 mm/d in the 200 m scenario. The flux is higher towards the production well and less significant on the opposite side, resulting in an unequal deformation (egg shape) of the injected bubble. This effect is less pronounced if the same production well is placed 400 m from the ASR well.

The alteration in mass concentration distribution arising from the extraction of the production well is discernible in the concentration breakthrough curves of the 1st and 5th cycles. This phenomenon imposes constraints on the maximum extraction volume due to the migration of freshwater from the storage zone. Conversely, the baseline scenario amplifies RE through cycling. Consequently, the discrepancies in RE become more pronounced with successive cycles.

The findings underscore a notable initial influence of dispersivity on the operational efficacy during the 1st cycle. Elevated dispersivity values escalate mixing owing to aquifer heterogeneity, leading to a broadening of the transition zone. Limited recovery concentration, coupled with constrained mixing fractions of injected and ambient water, resulted in the lower RE observed with higher dispersivity values. However, as cycle number increases, the impact on RE diminishes due to decreased concentrations in the storage zone. Higher dispersivity values benefit the most from reduced concentrations, resulting in a less prominent RE sensitivity in the 5th cycle compared to the 1st cycle. Brown (2005), Maliva (2020), and Merritt (1985, 1986) have also reported substantial effects.

The influence of aquifer thickness is exclusively evident in the case of a comparatively thin 60 m aquifer during the initial cycle. The ASR well screen penetrates the aquifer almost entirely in this scenario, limiting the expansion of the injection bubble towards the bottom. Initially, this setup results in limited mixing and slightly higher REs (82.8%) compared to the baseline scenario with a thicker 110 m aquifer (81.3%). However, this phenomenon diminishes over the long term. A thin, fully screened aquifer is deemed advantageous in reducing mixing in saline groundwaters, as suggested by Pyne (1995). Merritt (1985, 1986) also presents modelling results indicating a modest decrease in RE (6%) with increasing thickness of the most permeable zone.

The outcomes reveal a moderate sensitivity of effective porosity on RE during the 1st cycle, with a variation of 8% in the effective porosity range of 0.05–0.3. This aligns with findings by Merritt (1985, 1986), who reported a 7% change in RE in the range of 0.2–0.5. However, we found that this effect diminishes entirely with cycling.

Our results showed that specific storage and aquifer type do not exhibit effects on RE surpassing estimated uncertainties. Consequently, no significant sensitivity is discerned.

Initially, higher pumping rates appear to yield higher REs, but this effect diminishes over time. Merritt (1985, 1986) clarifies that large volumes (represented by high pump rates) exceeding 140,000 m^3 do not exhibit significant effects. Conversely, smaller volumes lead to a steady increase in RE with rising pump rates, emphasizing a nuanced relationship between pump rates and RE.

Heterogeneity in hydraulic conductivity manifests mass transport effects throughout the modelled period. While heterogeneity initially impacts RE, we found out that its significance diminishes with further cycling and has no discernible effects in the long run. Li et al. (2022) provide a detailed discussion on heterogeneity in hydraulic conductivity, affirming overall similar results.

Simulated TSV injection demonstrates that injecting an initial freshwater volume into the aquifer is effective in displacing groundwater from the storage zone and replacing it with high-quality water. The TSV reduces mixing with groundwater in successive cycles, directly enhancing ASR performance without requiring multiple cycles over several years. It is crucial to note that ASR operation post TSV injection should not exceed sustainable extraction to retain the TSV within the storage zone for subsequent cycles. Long-term RE analysis suggests that both baseline and TSV scenarios converge to a similar value of 112% after sufficient cycling. This behaviour holds true for TSV with ambient concentrations of 800 mg/l, showcasing that TSV injection is a viable recommendation in various settings where sufficient water is available.

The production well selected for ASR operation is predominantly constructed from wood and PVC, mitigating concerns about rust. The well is sealed with both technical and natural materials such as clay and sand, although the potential for upward flow during infiltration may not be entirely avoided. The technical condition of the production well is deemed satisfactory and ready for use. Although the screen does not cover the aquifer entirely, model results suggest that the impact is negligible. However, a more comprehensive analysis is warranted to understand the geological conditions around the screen and mitigate potential negative impacts.

5. Conclusion and outlook

The escalating challenges posed by urbanization, climate change, and the closure of production wells due to elevated sulphate concentrations in groundwater have intensified the need for effective water supply management. Particularly noteworthy are the difficulties encountered during summer months and extended drought periods, necessitating the establishment of additional water storage facilities.

This study explores a new option for using ASR as a cost-effective solution to store excess potable water in a low-quality aquifer by utilizing an existing well, thereby meeting peak demands during summer. The investigation focuses on a previously closed production well situated in a sulphate-rich aquifer, intended to serve as seasonal drinking water storage, effectively managing water resources and enhancing resilience. The core of this research involves the development and implementation of a numerical groundwater flow and mass transport model in FEFLOW 8.1. This model is meticulously designed to evaluate the impact of site-specific hydrogeological conditions and operational parameters on the long-term recovery efficiency (RE) of ASR in a brackish aquifer.

The numerical modelling results indicate that highly favourable REs exceeding 100% are achievable in suitable locations. However, several critical factors must be considered, including the hydraulic gradient in conjunction with hydraulic conductivity, injection and ambient concentrations, and dispersivity. Additionally, a designated operational mode termed target storage volume (TSV) is identified as highly valuable in diverse settings, expediting the establishment of long-term RE. The influence of various parameters on the model was significant in determining the efficiency and effectiveness of ASR. Hydraulic gradient played a major role, with steeper gradients causing more pronounced deformation and reduced recovery efficiency (RE). Ambient concentration impacted the breakthrough curves, with higher concentrations

resulting in steeper curves and increased RE over cycles. Injection concentration affected the speed of the concentration rise and influenced the RE, with lower injection concentrations achieving higher efficiencies. Dispersivity was found to delay the extraction process, with lower dispersivity leading to longer extraction durations. Effective porosity also affected water retention dynamics, with higher porosity leading to faster infiltration and less dispersion. Pumping rate influenced the infiltration and extraction volumes, with higher rates corresponding to larger transition zones and higher RE. Operational strategies like target volume storage (TSV) and the proximity of a neighbouring production well also had significant effects on RE, with TSV increasing the injected volume and RE, while the production well's proximity reduced efficiency, particularly at shorter distances.

The economic analysis conducted in the context of Hamburg metropolitan area indicates that ASR not only surpasses low-pressure reverse osmosis (LPRO) in cost-effectiveness but also presents an avenue for enhancing resilience to climate change. ASR achieves this by effectively storing surplus water during periods of high availability and subsequently filling the supply deficit during periods of heightened demand or drought. In contrast, LPRO is constrained by the prerequisite of sufficient water availability for treatment and the presence of a suitable means for the disposal of concentrate. Moreover, LPRO faces operational limitations, being particularly vital during high-demand summer months but potentially inactive in winter when existing capacity adequately meets demand. Additionally, ASR exhibits superior water usage efficiency compared to LPRO membranes, as it necessitates the disposal of only 20% of the concentrate.

Our study indicates that ASR implementation in low-quality aquifers holds significant promise in terms of environmental and economic viability, particularly in urban settings such as Hamburg. To apply this framework to other regions, a comprehensive analysis of ASR utilizing production wells is imperative. Detailed scrutiny of well design, geological assessment of subsurface conditions to ascertain feasibility, and the development of a more realistic study area model are essential components of this analysis. For an in-depth exploration of well design and potential geochemical interactions, Pyne's (1995) book is recommended. Evaluation of the existing well's condition should involve video camera logging, wire brushing of the screen and casing, acid treatment, and disinfection prior to testing. Furthermore, integrating ASR into the regional model, specifically as a seasonal storage mechanism, is crucial for understanding localized effects, determining recovery efficiency, and establishing overall feasibility (Sallam, 2019). The incorporation of reactive transport modelling within the model, although requires huge effort, is essential to simulate processes like the oxidation of pyrite, soil organic matter (SOM), and ferrous iron (Antoniou et al., 2013). Upon confirmation of feasibility, the consideration of a pilot test project using a production well becomes paramount. This pilot initiative should adhere to a well-structured framework, as outlined by Brown (2005). Additionally, insights from Australian guidelines for Water Recycling, 2009 (NRMMC, ERHC and NHMRC, 2009) can offer valuable guidance and lessons for the implementation of Managed Aquifer Recharge (MAR). Utilizing dimensionless parameters proposed by Ward et al. (2007, 2008, 2009) during the early planning stages can contribute feasibility factors to the project.

During the pilot testing phase, addressing challenges such as clogging is crucial for effective management. Prior research, summarized by Pyne (1995), identifies five processes contributing to clogging: gas binding, deposition of total suspended solids, biological growth, geochemical reactions, and particle rearrangement in aquifer materials. The impact of these processes on well plugging is contingent on site-specific conditions (aquifer and groundwater characteristics), well construction, and source water quality. Considering and mitigating these processes is essential for ensuring the long-term success of the ASR operation.

A thorough consideration of the inherent limitations of the model in scenario-based modelling within the framework of this study, particularly when extrapolating its application to other regions is imperative. The validity of model predictions depends on several critical factors, including the precision and coherence of the assigned spatio-temporal resolution and mesh configuration, the representation of aquifer heterogeneity, the scale of the model domain, as well as the accuracy of boundary and initial conditions.

6. Framework implementation: investigating feasibility factors and operational strategies

In this section, we summarize the technical and decision-making components within our framework, aimed at offering recommendations tailored for urban planners and policymakers.

6.1. Location data for ASR feasibility assessment

Essential data parameters include water supply/demand dynamics, monthly extraction rates from wells over extended periods, technical utilization rates per annum for production wells, legal extraction constraints, drinking water quality standards, water demand projections, and infrastructure details such as well construction specifics, availability of freshwater sources, treatment plant capacities, and utilization rates. Aquifer hydrogeological considerations encompass geological assessments, outcomes of pumping and tracer tests, and requisite aquifer data for modelling, including hydraulic head measurements and concentrations of pertinent dissolved salts, ensuring injection water quality complies with drinking water standards.

6.2. Water supply and demand analysis

A comprehensive analysis of future water demand is imperative, considering urbanization trends, environmental factors, and anticipated impacts of climate change. Assurance of adequate water supply, both in terms of quality and quantity, is fundamental. Variations in monthly water quality and quantity necessitate careful planning of treatment strategies and optimization of recharge and recovery phases and volumes, particularly in semi-arid regions where rainwater harvesting may offer a supplemental water source.

6.3. Infrastructure assessment

Leveraging existing infrastructure to minimize capital outlay is crucial, with close proximity to treatment facilities and potential repurposing of idle pipelines and production wells offering cost-effective solutions. Thoroughly checking the design and technical details is crucial to ensure operational viability, including the selection of corrosion-resistant casing materials and mitigation of potential clogging risks associated with inadequate sealing.

6.4. Hydrogeology evaluation

Thorough assessment of critical hydrogeological parameters is imperative for optimizing ASR efficiency. Considerations include hydraulic gradient analysis, accurate estimation of hydraulic conductivity through pumping tests, and evaluation of dispersivity via tracer studies. Spatial and temporal variability in concentration levels, as well as potential impacts from neighbouring production wells, must be carefully examined to inform effective ASR implementation.

6.5. Development of numeric groundwater model

Integration of previously collected and analysed data into a conceptual design forms the basis for developing a numerical groundwater model using software tools like FEFLOW. Attention to model discretization ensures stability and accuracy, with quantification of uncertainties and sensitivity analyses aiding in model validation and

refinement.

6.6. Performing sensitivity analysis

Sensitivity analyses on key parameters provide valuable insights into ASR feasibility, necessitating rigorous testing and validation of assumptions. Utilization of computational tools, expedites the analysis process, while exploration of alternate operational modes can potentially enhance overall recovery efficiency.

6.7. Development of operational guidelines

Insights gained from sensitivity analyses inform the development of operational guidelines, guiding decisions regarding technical storage volumes and maximum storage durations to optimize ASR performance and ensure successful implementation.

CRediT authorship contribution statement

Vahid Sobhi Gollo: Writing – review & editing, Writing – original draft, Visualization, Supervision, Software, Methodology, Investigation, Formal analysis, Conceptualization. **Bentley Bo Schmidt:** Writing – review & editing, Writing – original draft, Visualization, Validation, Software, Resources, Methodology, Investigation, Formal analysis, Data curation. **Carsten Hansen:** Writing – review & editing, Supervision, Resources, Methodology, Formal analysis, Conceptualization. **Nima Shokri:** Writing – review & editing, Supervision, Methodology, Formal analysis, Conceptualization.

Declaration of generative AI and AI-assisted technologies in the writing process

During the preparation of this work the authors used ChatGPT 3.5 for proofreading the text. After using this tool, the authors reviewed and edited the content as needed and take full responsibility for the content of the publication.

Declaration of competing interest

The authors declare that they have no known competing financial interests or personal relationships that could have appeared to influence the work reported in this paper.

Acknowledgements

This research initiative is a collaborative endeavor between Consulaqua, a subsidiary of Hamburg Wasser (Hamburg Waterworks), and the Hamburg University of Technology. Our appreciation is extended to Hamburg Wasser for furnishing essential data pertaining to the hydrogeological structure, water quality, consumption patterns, and well characteristics. Additionally, we express gratitude to BUKEA (Hamburg office for the Environment, Climate, Energy and Agriculture) for their support in providing hydraulic data for the designated study region.

Appendix A. Supplementary data

Supplementary data to this article can be found online at https://doi.org/10.1016/j.gsd.2024.101396.

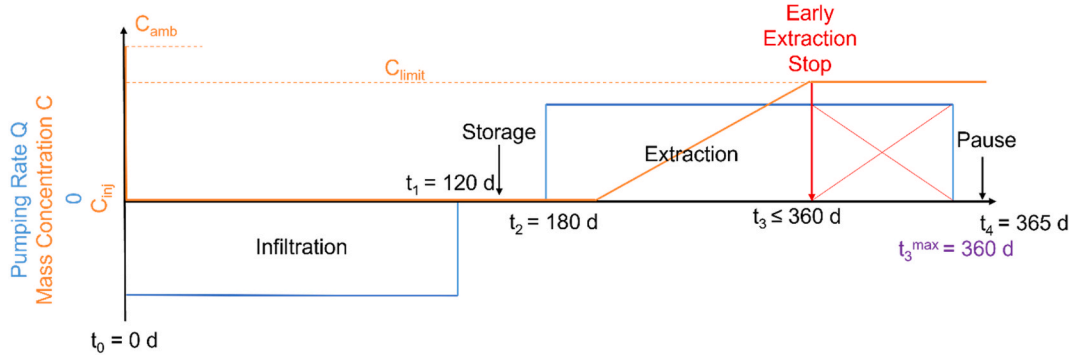

Figure A1. Schematic overview of the ASR approach employed in this study. The blue components represent the Well Boundary Conditions (Well BC), while the orange components depict the Mass Boundary Conditions (Mass BC).

Data availability

Data will be made available on request.

References

Alcamo, J., 2019. Water quality and its interlinkages with the sustainable development goals. Curr. Opin. Environ. Sustain. 36, 126–140. https://doi.org/10.1016/j.cosust.2018.11.005.

Aminzadeh, M., Friedrich, N., Narayanaswamy, S.G., Madani, M., Shokri, N., 2024. Evaporation loss from small agricultural reservoirs: an overlooked component of water accounting. Earth's Future 12, e2023EF004050. https://doi.org/10.1029/2023EF004050.

Aminzadeh, M., Or, D., Stevens, B., AghaKouchak, A., Shokri, N., 2023. Upper bounds of maximum land surface temperatures in a warming climate and limits to plant growth. Earth's Future 11, e2023EF003755. https://doi.org/10.1029/2023EF003755.

Antoniou, A., Smits, F., Stuyfzand, P., 2017. Quality assessment of deep-well recharge applications in The Netherlands. Water Supply 17, 1201–1211. https://doi.org/10.2166/ws.2017.032.

Antoniou, E.A., Stuyfzand, P.J., Van Breukelen, B.M., 2013. Reactive transport modeling of an aquifer storage and recovery (ASR) pilot to assess long-term water quality improvements and potential solutions. Appl. Geochem. 35, 173–186. https://doi.org/10.1016/j.apgeochem.2013.04.009.

Ashbolt, N.J., 2004. Microbial contamination of drinking water and disease outcomes in developing regions. Toxicology 198, 229–238. https://doi.org/10.1016/j.tox.2004.01.030.

Bhaduri, A., Bogardi, J., Siddiqi, A., Voigt, H., Vörösmarty, C., Pahl-Wostl, C., Bunn, S.E., Shrivastava, P., Lawford, R., Foster, S., Kremer, H., Renaud, F.G., Bruns, A., Osuna, V.R., 2016. Achieving sustainable development goals from a water perspective. Front. Environ. Sci. 4. https://doi.org/10.3389/fenvs.2016.00064.

Brindha, K., Schneider, M., 2019. Impact of urbanization on groundwater quality. In: Venkatramanan, S., Prasanna, M.V., Chung, S.Y. (Eds.), GIS and Geostatistical Techniques for Groundwater Science. Elsevier, pp. 179–196. https://doi.org/10.1016/B978-0-12-815413-7.00013-4.

Broere, W., 2016. Urban underground space: solving the problems of today's cities. Tunn. Undergr. Space Technol. 55, 245–248. https://doi.org/10.1016/j.tust.2015.11.012.

Brown, C., 2005. Planning Decision Framework for Brackish Water Aquifer Storage and Recovery (ASR) Projects (Dissertation). University of Florida, Florida.
BUKEA, 2020. Geological map of the state bureau of the environment, climate, energy and agriculture of Hamburg, Germany. https://geoportal-hamburg.de/bohrdaten/index.html.
Choi, J., Skibniewski, M., Shim, Y.-G., 2017. Economics of alternative water resources with an emphasis on aquifer storage and recovery. Water Supply 18, 612–621. https://doi.org/10.2166/ws.2017.137.
Diersch, H.-J.G., 2014. FEFLOW: Finite Element Modeling of Flow, Mass and Heat Transport in Porous and Fractured Media. Springer Berlin Heidelberg, Berlin, Heidelberg. https://doi.org/10.1007/978-3-642-38739-5.
Dillon, P., 2009. Managed aquifer recharge: an introduction. In: National Water Commission. A.C.T, Canberra.
Dillon, P., Alley, W., Zheng, Y., Vanderzalm, J., Page, D., Ward, J., Megdal, S., Hipke, W., Thomas, P., Tuthill, D., Carlson, R., 2022. Managed aquifer recharge: overview and governance. International Association of Hydrogeologists.
Dillon, Peter, Forster, S., Scanlon, B.R., Stigter, T.Y., 2019b. Climate-change adaption and groundwater. Strategic Overview Series. IAH.
Dillon, P., Stuyfzand, P., Grischek, T., Lluria, M., Pyne, R.D.G., Jain, R.C., Bear, J., Schwarz, J., Wang, W., Fernandez, E., Stefan, C., Pettenati, M., van der Gun, J., Sprenger, C., Massmann, G., Scanlon, B.R., Xanke, J., Jokela, P., Zheng, Y., Rossetto, R., Shamrukh, M., Pavelic, P., Murray, E., Ross, A., Bonilla Valverde, J.P., Palma Nava, A., Ansems, N., Posavec, K., Ha, K., Martin, R., Sapiano, M., 2019a. Sixty years of global progress in managed aquifer recharge. Hydrogeol. J. 27, 1–30. https://doi.org/10.1007/s10040-018-1841-z.
European Parliament, Council of the European Union, 2021. Directive (EU) 2020/2184 of the European Parliament and of the Council of 16 December 2020 on the Quality of Water Intended for Human Consumption, p. 2184.
Falgout, R.D., 2006. An introduction to algebraic multigrid. Comput. Sci. Eng. 8, 24–33. https://doi.org/10.1109/MCSE.2006.105.
Goderniaux, P., Brouyère, S., Wildemeersch, S., Therrien, R., Dassargues, A., 2015. Uncertainty of climate change impact on groundwater reserves – application to a chalk aquifer. J. Hydrol. 528, 108–121. https://doi.org/10.1016/j.jhydrol.2015.06.018.
Goel, M., 2021. Groundwater pollution by geogenic and industrial pollutants. In: Gupta, P.K., Bharagava, R.N. (Eds.), Fate and Transport of Subsurface Pollutants. Springer Singapore, Singapore, pp. 21–33. https://doi.org/10.1007/978-981-15-6564-9_2.
Hajek, O.L., Knapp, A.K., 2022. Shifting seasonal patterns of water availability: ecosystem responses to an unappreciated dimension of climate change. New Phytol. 233, 119–125. https://doi.org/10.1111/nph.17728.
Hemenway, C., Grundemannz, P. (Eds.), 2002. ASR as a Water Management Tool for Highlands Ranch, Colorado, in: Ground Water/Surface Water Interactions, American Water Resources Association Technical Publication Series. Presented at the AWRA 2002 Summer Specialty Conference, American Water Resources Association, Keystone, Colorado.
Henao Casas, J.D., Fernández Escalante, E., Ayuga, F., 2022. Alleviating drought and water scarcity in the Mediterranean region through managed aquifer recharge. Hydrogeol. J. 30 (6), 1685–1699.
Himmel, M., Schäfer, W., 2010. Hinweise zur Erstellung und Beurteilung von Grundwassermodellen im Altlastenbereich (No. 12), LANUV-Arbeitsblatt. LANUV NRW, Recklinghausen.
Hossain, Md I., Bari, Md N., Miah, S.U., Jahan, C.S., Rahaman, Md F., 2020. Performance of MAR model for stormwater management in Barind Tract, Bangladesh. Groundwater for Sustainable Development 10, 100285. https://doi.org/10.1016/j.gsd.2019.100285.
Ibrahim, M.B., 2009. Rainwater harvesting for urban areas: a success story from gadarif city in Central Sudan. Water Resour. Manag. 23 (13), 2727–2736. https://doi.org/10.1007/s11269-009-9405-6.
Jéquier, E., Constant, F., 2010. Water as an essential nutrient: the physiological basis of hydration. Eur. J. Clin. Nutr. 64, 115–123. https://doi.org/10.1038/ejcn.2009.111.
Jha, R., Singh, V.P., Singh, V., Roy, L.B., Thendiyath, R. (Eds.), 2022. Groundwater and Water Quality: Hydraulics, Water Resources and Coastal Engineering, Water Science and Technology Library. Springer International Publishing, Cham. https://doi.org/10.1007/978-3-031-09551-1.
Kolditz, O., Ratke, R., Diersch, H.-J.G., Zielke, W., 1998. Coupled groundwater flow and transport: 1. Verification of variable density flow and transport models. Adv. Water Resour. 21, 27–46. https://doi.org/10.1016/S0309-1708(96)00034-6.
Kumar, M., Deka, J.P., Kumari, O., 2020. Development of Water Resilience Strategies in the context of climate change, and rapid urbanization: a discussion on vulnerability mitigation. Groundwater for Sustainable Development 10, 100308. https://doi.org/10.1016/j.gsd.2019.100308.
Lall, U., Josset, L., Russo, T., 2020. A snapshot of the world's groundwater challenges. Annu. Rev. Environ. Resour. 45, 171–194. https://doi.org/10.1146/annurev-environ-102017-025800.
Li, H., Lu, C., Werner, A.D., Irvine, D.J., Luo, J., 2022. Impacts of heterogeneity on aquifer storage and recovery in saline aquifers. Water Resour. Res. 58. https://doi.org/10.1029/2021WR031306.
Lluria, M.R., Paski, P.M., Small, G.G., 2018. Seasonal water storage and replenishment of a fractured granitic aquifer using ASR wells. Sustainable Water Resources Management 4, 261–274. https://doi.org/10.1007/s40899-018-0233-9.
Lu, C., Du, P., Chen, Y., Luo, J., 2011. Recovery efficiency of aquifer storage and recovery (ASR) with mass transfer limitation. Water Resour. Res. 47. https://doi.org/10.1029/2011WR010605.
Malik, R.S., Yadav, D.K., Jhorar, B.S., Jhorar, R.K., Streck, T., 2006. Physical and chemical interactions in an ASR cavity well in a brackish aquifer. Recharge Systems for Protecting and Enhancing Groundwater Resources, pp. 120–125.
Maliva, R.G., 2020. Anthropogenic Aquifer Recharge: WSP Methods in Water Resources Evaluation Series No. 5, Springer Hydrogeology. Springer, Cham. https://doi.org/10.1007/978-3-030-11084-0.
Maliva, R.G., Manahan, W.S., Missimer, T.M., 2019. Aquifer storage and recovery using saline aquifers: hydrogeological controls and opportunities. Groundwater 58, 9–18. https://doi.org/10.1111/gwat.12962.
Manhenke, V., Reutter, E., Hübschmann, M., Limberg, A., Lückstädt, M., Nommensen, B., Peters, A., Schlimm, W., Tauks, R., Voigt, H.-J., 2001. Hydrostratigraphic division of the Pleistocene and Holocene unconsolidated rock area of northern and central Germany. Hannover (BGR).
Mannan, M., Al-Ansari, T., Mackey, H.R., Al-Ghamdi, S.G., 2018. Quantifying the energy, water and food nexus: a review of the latest developments based on life-cycle assessment. J. Clean. Prod. 193, 300–314. https://doi.org/10.1016/j.jclepro.2018.05.050.
Merritt, M.L., 1986. Recovering fresh water stored in saline limestone aquifers. Ground Water 24, 516–529. https://doi.org/10.1111/j.1745-6584.1986.tb01031.x.
Merritt, M.L., 1985. Subsurface storage of freshwater in South Florida: a digital model analysis of recoverability (Report No. 2261). Water Supply Paper. https://doi.org/10.3133/wsp2261.
Moravec, V., Markonis, Y., Rakovec, O., Svoboda, M., Trnka, M., Kumar, R., Hanel, M., 2021. Europe under multi-year droughts: how severe was the 2014–2018 drought period? Environ. Res. Lett. 16, 034062. https://doi.org/10.1088/1748-9326/abe828.
Murray Ricky, Tredoux G., Botha, F., 2005. Artificial groundwater recharge : wise water management for towns and cities. IMIESA 30, 20–27. https://doi.org/10.10520/EJC43543.
Nrmmc, E.R.H.C., Nhmrc, 2009. Australian Guidelines for Water Recycling: Managed Aquifer Recharge (National Water Quality Management Strategy No. 24); Natural Resource Management Ministerial Council (NRMMC). Environment Protection and Heritage Council (ERHC) and National Health and Medical Research Council (NHMRC), Canberra, Australia.
Pimentel, D., Berger, B., Filiberto, D., Newton, M., Wolfe, B., Karabinakis, E., Clark, S., Poon, E., Abbett, E., Nandagopal, S., 2004. Water resources: agricultural and environmental issues. Bioscience 54, 909–918. https://doi.org/10.1641/0006-3568(2004)054[0909:WRAAEI]2.0.CO;2.
Posey, H.H., Kyle, J.R., 1988. Fluid-rock interactions in the salt dome environment: an introduction and review. Chem. Geol. 74, 1–24. https://doi.org/10.1016/0009-2541(88)90143-X.
Postel, S.L., 2000. Entering an era of water scarcity: the challenges ahead. Ecol. Appl. 10, 941–948. https://doi.org/10.1890/1051-0761(2000)010[0941:EAEOWS]2.0.CO;2.
Pyne, R.D.G., 2014. The economics of aquifer storage recovery technology. Bol. Geol. Min. 125, 219–225.
Pyne, R.D.G., 1995. Groundwater Recharge and Wells: A Guide to Aquifer Storage Recovery, first ed. LEWIS, Boca Raton. https://doi.org/10.1201/9780203719718.
Pyne, R.D.G., President, P., 2003. Water quality in aquifer storage recovery (ASR) wells. In: Presented at the Annual Meeting of the American Water Works Association (Florida Section). Orlando: American Water Works Association.
Reese, R.S., 2002. Inventory and Review of Aquifer Storage and Recovery in Southern Florida (Report No. 2002–4036). Water-Resources Investigations Report, Reston, VA. https://doi.org/10.3133/wri024036.
Rinck-Pfeiffer, S., Pitman, C., Dillon, P., 2006. Stormwater ASR in Practice and ASTR under Investigation in Salisbury, South Australia, in: Recharge Systems for Protecting and Enhancing Groundwater Resources. 5th International Symposium on Management of Aquifer Recharge (ISMAR), Berlin, Germany, pp. 151–159, 2005.
Sallam, O.M., 2019. Use of numerical groundwater modeling to assess the feasibility of aquifer storage and recovery (ASR) in the wadi watir delta, sinai, Egypt. JWARP 11, 1462–1480. https://doi.org/10.4236/jwarp.2019.1112085.
Seiler, K.-P., Gat, J.R., 2007. Groundwater recharge from run-off. Infiltration and Percolation, Water Science and Technology Library. Springer, London, Dortrecht, Netherlands.
Sharma, M.K., Kumar, M., 2020. Sulphate contamination in groundwater and its remediation: an overview. Environ. Monit. Assess. 192, 74. https://doi.org/10.1007/s10661-019-8051-6.
Stefan, C., Ansems, N., 2018. Web-based global inventory of managed aquifer recharge applications. Sustain. Water Resour. Manag. 4, 153–162. https://doi.org/10.1007/s40899-017-0212-6.
Suhag, R., 2016. Overview of Ground Water in India. PRS. https://www.jstor.org/stable/24111024.
Taneja, D.S., Khepar, S.D., 1996. Effect of artificial ground-water recharge on aquifer parameters using cavity well. Groundwater 34 (2), 335–340. https://doi.org/10.1111/j.1745-6584.1996.tb01893.x.
Tuinhof, A., Heederik, J.P., 2002. Management of aquifer recharge and subsurface storage : making better use of our largest reservoir. Seminar, Wageningen 18–19. December 2002. ISBN 90-808258-1-6.
UN General Assembly, 2015. *Transforming our world: the 2030 Agenda for Sustainable Development*, 21 October 2015, A/RES/70/1. available at: https://www.refworld.org/docid/57b6e3e44.html. (Accessed 6 November 2023).
United Nations, 2023. The Sustainable Development Goals Report 2023, Special edition. United Nations. https://unstats.un.org/sdgs/report/2023/The-Sustainable-Development-Goals-Report-2023.pdf.
Velis, M., Conti, K.I., Biermann, F., 2017. Groundwater and human development: synergies and trade-offs within the context of the sustainable development goals. Sustain. Sci. 12, 1007–1017. https://doi.org/10.1007/s11625-017-0490-9.

Ward, J.D., Simmons, C.T., Dillon, P.J., 2008. Variable-density modelling of multiple-cycle aquifer storage and recovery (ASR): importance of anisotropy and layered heterogeneity in brackish aquifers. J. Hydrol. 356, 93–105. https://doi.org/10.1016/j.jhydrol.2008.04.012.

Ward, J.D., Simmons, C.T., Dillon, P.J., 2007. A theoretical analysis of mixed convection in aquifer storage and recovery: how important are density effects? J. Hydrol. 343, 169–186. https://doi.org/10.1016/j.jhydrol.2007.06.011.

Ward, J.D., Simmons, C.T., Dillon, P.J., Pavelic, P., 2009. Integrated assessment of lateral flow, density effects and dispersion in aquifer storage and recovery. J. Hydrol. 370, 83–99. https://doi.org/10.1016/j.jhydrol.2009.02.055.

Wendler, B., Stumme, J., Ernst, M., Sperlich, A., Benne, P., Gnirß, R., Mergel, D., Ernst, S., Jährig, J., Conzelmann, L., Remy, C., Miehe, U., Niestroj-Pahl, R., Dähne, L., Krug, M., Heijnen, M., 2022. SULEMAN - Aufbereitung von Grundwässern mit erhöhtem Sulfatgehalt: Innovative Optionen und Grenzen eines ressourcen- und insbesondere energieeffizienten Trinkwassermanagements: gemeinsamer Abschlussbericht der Verbundprojektpartner: Grundwasser Sulfat Anaerobe Aufbereitung LPRO Membranmodifikation CARIX LCA : Laufzeit: 01.06.2018 bis 28.02.2022. DVGW. https://doi.org/10.2314/KXP:1844958981.

Whitehead, W., 1974. Storage of Fresh Water in Saline Aquifers Using a Well Field. Louisiana State University and Agricultural and Mechanical College. https://doi.org/10.31390/gradschool_disstheses.2704 (Doctor of Philosophy).

WHO, 2023. Drinking water [document]. URL. https://www.who.int/news-room/fact-sheets/detail/drinking-water.

Williams, A.I.L., O'Gorman, P.A., 2022. Summer-winter contrast in the response of precipitation extremes to climate change over northern hemisphere land. Geophys. Res. Lett. 49, e2021GL096531. https://doi.org/10.1029/2021GL096531.

Woessner, W.W., Poeter, E.P., 2020. Hydrogeologic Properties of Earth Materials and Principles of Groundwater Flow. The Groundwater Project, Guelph, Ontario, Canada.

Zech, A., Attinger, S., Cvetkovic, V., Dagan, G., Dietrich, P., Fiori, A., Rubin, Y., Teutsch, G., 2015. Is unique scaling of aquifer macrodispersivity supported by field data? Water Resour. Res. 51, 7662–7679. https://doi.org/10.1002/2015WR017220.

Zheng, Y., Ross, A., Villholth, K.G., Dillon, P., 2021. Managing Aquifer Recharge: A Showcase for Resilience and Sustainability. (UNESCO, Ed.). UNESCO. https://unesdoc.unesco.org/ark:/48223/pf0000379962.locale=en.